HHS Public Access

Author manuscript

Cell Chem Biol. Author manuscript; available in PMC 2025 February 15.

Published in final edited form as:

Cell Chem Biol. 2024 February 15; 31(2): 234–248.e13. doi:10.1016/j.chembiol.2023.10.011.

Sensitization of Cancer Cells to Ferroptosis Coincident with Cell Cycle Arrest

Jason Rodencal[1], **Nathan Kim**[1], **Andrew He**[2], **Veronica L. Li**[3], **Mike Lange**[4,5], **Jianping He**[6], **Amy Tarangelo**[1], **Zachary T. Schafer**[6], **James A. Olzmann**[4,5,7], **Jonathan Z. Long**[3], **Julien Sage**[2], **Scott J. Dixon**[1,8,*]

[1]Department of Biology, Stanford University, Stanford, CA 94305, USA

[2]Departments of Pediatrics and Genetics, Stanford University School of Medicine, Stanford, CA 94305, USA

[3]Department of Pathology, Stanford University School of Medicine, Stanford, CA 94305, USA

[4]Department of Molecular and Cell Biology, University of California, Berkeley, Berkeley, CA 94720, USA

[5]Department of Nutritional Sciences and Toxicology, University of California, Berkeley, Berkeley, CA 94720, USA

[6]Department of Biological Sciences, University of Notre Dame, Notre Dame, IN 46556, USA

[7]Chan Zuckerberg Biohub, San Francisco, CA 94158, USA

[8]Lead contact

SUMMARY

Ferroptosis is a non-apoptotic form of cell death that can be triggered by inhibiting the system x_c^- cystine/glutamate antiporter or the phospholipid hydroperoxidase glutathione peroxidase 4 (GPX4). We have investigated how cell cycle arrest caused by stabilization of p53 or inhibition of cyclin-dependent kinase 4/6 (CDK4/6) impacts ferroptosis sensitivity. Here, we show that cell cycle arrest can enhance sensitivity to ferroptosis induced by covalent GPX4 inhibitors (GPX4i) but not system x_c^- inhibitors. Greater sensitivity to GPX4i is associated with increased levels of oxidizable polyunsaturated fatty acid-containing phospholipids (PUFA-PLs). Higher PUFA-PL abundance upon cell cycle arrest involves reduced expression of membrane bound

*Correspondence: sjdixon@stanford.edu.

AUTHOR CONTRIBUTIONS

Conceptualization, J.R., M.L., J.H., A.T., Z.T.S., J.A.O., J.Z.L., J.S., S.J.D.; Methodology, J.R., V.L.L., A.H., M.L., J.H., A.T.; Investigation, J.R., N.K., V.L.L., A.H., M.L., J.H., A.T.; Writing, J.R., and S.J.D.; Funding Acquisition and Supervision, Z.T.S., J.A.O., J.Z.L., J.S., and S.J.D.

DECLARATION OF INTERESTS

J.A.O. is a member of the scientific advisory board for Vicinitas Therapeutics and an inventor on ferroptosis-related patent applications. S.J.D. is a co-founder of Prothegen Inc., a member of the scientific advisory board of Ferro Therapeutics and Hillstream Biopharma, and an inventor on patents related to ferroptosis.

O-acyltransferase domain containing 1 (*MBOAT1*) and epithelial membrane protein 2 (*EMP2*). A candidate orally bioavailable GPX4 inhibitor increases lipid peroxidation and shrinks tumor volumes when combined with a CDK4/6 inhibitor. Thus, cell cycle arrest may make certain cancer cells more susceptible to ferroptosis in vivo.

Graphical Abstract

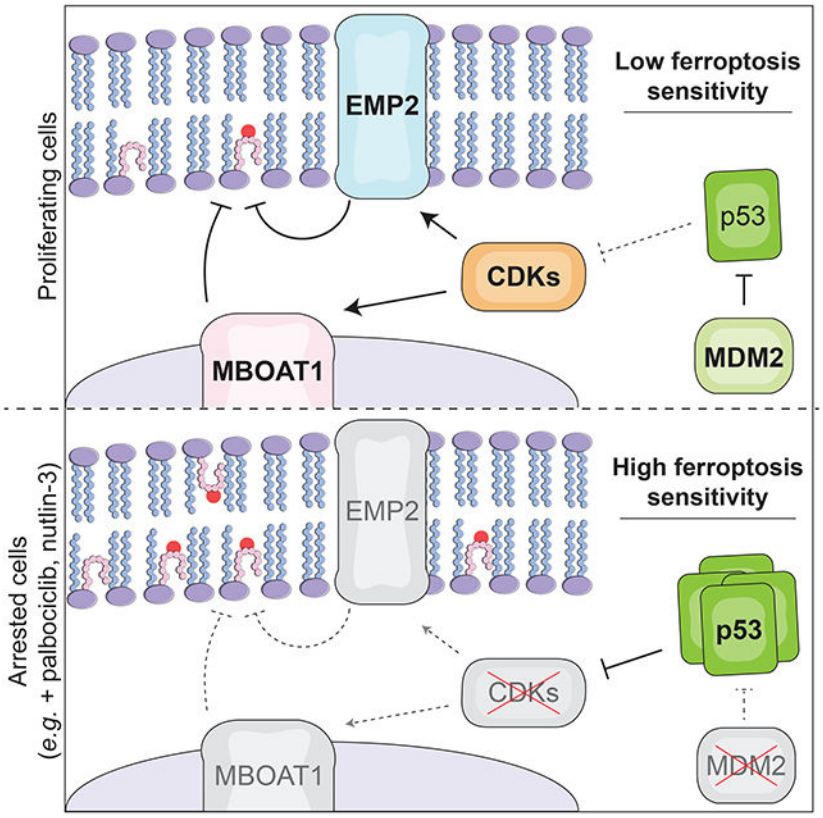

eTOC:

Ferroptosis regulation remains poorly understood. Rodencal et al. demonstrate that cell cycle arrest enhances sensitivity to ferroptosis when this process is induced by direct inhibition of GPX4. It may be possible to target this mechanism in vivo using growth arresting agents together with an orally bioavailable GPX4 inhibitor.

Keywords

lipid peroxidation; ferroptosis; p53; MBOAT1; EMP2; MUFA; PUFA; palbociclib; CDK4/6

INTRODUCTION

Ferroptosis is a non-apoptotic cell death mechanism that may be exploitable for cancer therapy.[1,2] Ferroptosis can be triggered by inhibition of the plasma membrane cystine/glutamate antiporter system x_c^- or the glutathione-dependent lipid hydroperoxidase

glutathione peroxidase 4 (GPX4).[3-5] Small molecule inhibitors of system x_c^- (e.g., erastin) and GPX4 (e.g., RSL3 and ML210) cause the lethal accumulation of membrane phospholipid hydroperoxides.[6-10] However, cystine deprivation and direct GPX4 inhibition cause ferroptosis through related yet distinct mechanisms.[11] For example, the polyunsaturated fatty acid (PUFA) metabolic enzyme acyl-CoA synthetase long chain family member 4 (ACSL4) may be more important for ferroptosis caused by direct GPX4 inhibition than by system x_c^- inhibition or other stimuli.[11-13] Molecular mechanisms that govern these distinct forms of ferroptosis remain poorly understood.

p53 is a transcription factor that can regulate diverse targets involved in cell cycle regulation, cell death, metabolism and other processes.[14,15] We and others find that stabilization of wild type p53 in human cancer cells can reduce sensitivity to ferroptosis triggered by system x_c^- inhibition.[16-18] Mechanistically, reduced ferroptosis sensitivity in this context may involve altered protease function or the conservation of intracellular glutathione. The p53-inducible gene product cyclin dependent kinase inhibitor 1A (CDKN1A, p21) may also influence GPX4 inhibitor sensitivity, either downstream of p53 or independently.[18-20] Among other functions, p53 and CDKN1A can arrest cell cycle progression. The cell cycle-associated genes *CDKN2A* and *RB1* are also linked to the regulation of ferroptosis sensitivity[19,21]. Molecular mechanisms that explain how the cell cycle influences ferroptosis sensitivity require further elucidation.

Here, we investigated how wild type p53 expression impacts ferroptosis sensitivity. We find that wild type p53 expression has two distinct effects on ferroptosis: suppression of ferroptosis in response to system x_c^- inhibition and sensitization to ferroptosis in response to direct GPX4 inhibitors. We link sensitization to GPX4 inhibitors to cyclin dependent kinase (CDK) inhibition, cell cycle arrest, reduced expression of the lipid metabolic gene *MBOAT1* and the tetraspanin *EMP2*, and altered levels of oxidizable polyunsaturated phosphatidylethanolamine (PUFA-PE) plasmalogens. We show that cell cycle arrest combined with GPX4 inhibition may enhance tumor cell lipid peroxidation in vivo. These results uncover a mechanistic link between the cell cycle and ferroptosis sensitivity via EMP2-dependent changes in lipid metabolism.

RESULTS

A screen for modulators of cell death upon p53 expression

Stabilization of wild type p53 can enhance resistance to ferroptosis caused by system x_c^- inhibition.[16-18] We were initially curious whether p53-stabilized cells responded in a similar manner to other lethal stimuli and designed a small molecule screen to examine this question (Figure 1A). Wild type p53 accumulates after treatment with the MDM2 inhibitor nutlin-3 (10 μM, 48 h).[16] Because p53 expression itself can arrest cell proliferation, in this and all other experiments cells were seeded initially at densities that ensured a similar number of cells in both the control and nutlin-3-treated populations after 48 h. We then exposed these cells to 261 mechanistically diverse compounds, including kinase inhibitors, epigenetic modulators, and known inducers of different forms of cell death[8], and measured cell death using the scalable time-lapse analysis of cell death kinetics (STACK) imaging method.[22]

The lethality of each compound was compared between cells pretreated with nutlin-3 versus DMSO (Figure 1A).

As observed previously,[16-18] p53 stabilization conferred resistance to the structurally similar small molecule system x_c^- inhibitors erastin and erastin2, a result confirmed in focused assays using the same conditions (Figures 1B, 1C, and Data S1). Also as expected, p53 stabilization resulted in greater sensitivity to the pro-apoptotic BCL-2/BCL-xL inhibitors ABT-737 and A-1331852 (Figure 1B).[23] Unexpectedly, p53-stabilized cells were also sensitized to the covalent GPX4 inhibitors (GPX4i) RSL3 and ML162, a result we confirmed in focused assays (Figures 1B and 1C). Stabilization of wild type p53 also reduced sensitivity to erastin2 while increasing sensitivity to RSL3 in Caki-1 renal carcinoma and A375 melanoma cells, consistent with a generalizable effect (Figures S1A and S1B). By contrast, decreased sensitivity to erastin2 and increased sensitivity to RSL3 were not observed in an established[16] HT-1080 p53 gene disrupted (i.e., $p53^{KO}$) cell line pretreated for 48 h with nutlin-3 (Figure 1C). Consistent with a p53-independent role for MDM2 in ferroptosis regulation,[18,24] nutlin-3 pre-treatment enhanced erastin2 sensitivity in HT-1080 $p53^{KO}$ cells (Figure 1C), but this weak effect was not investigated further. Collectively, these findings indicated that p53 stabilization could confer resistance to ferroptosis triggered by system x_c^- inhibition and simultaneously enhance sensitivity to ferroptosis caused by direct GPX4 inhibition.

Cell cycle arrest correlates with GPX4i sensitization

Wild type p53 can suppress ferroptosis induced by system x_c^- inhibition by enhancing glutathione levels or by modulating other targets.[16,17,25] How p53 expression sensitized to small molecule GPX4i was less clear, prompting us to investigate further. p53 has numerous transcriptional targets, including *CDKN1A*. CDKN1A can regulate CDK2, CDK4, and CDK6, which in turn control G1/S progression via inhibition of the retinoblastoma (RB) tumor suppressor (Figure 1D).[26] We tested the hypothesis that CDK4/6 inhibition was sufficient to sensitize to GPX4i by pretreating Control and $p53^{KO}$ HT-1080^N cells with the CDK4/6 inhibitor palbociclib (2 μM, 48 h).[27] Strikingly, both Control and $p53^{KO}$ cells pretreated with palbociclib for 48 h were sensitized to RSL3 but not erastin2 (Figure 1C). Palbociclib treatment inhibited cell cycle progression in both Control and $p53^{KO}$ cells as judged by reduced Rb phosphorylation, reduced *E2F1* expression, and cell cycle arrest at the G1/S transition, while nutlin-3 had these effects only in Control cells (Figures 1E-1G). Palbociclib pretreatment likewise reduced the expression of Rb-regulated cell cycle genes (*E2F1, CCNA2*) and selectively sensitized to RSL3 but not erastin2 in Caki-1 and A375 cells, without altering p53 levels (Figures S1A-S1F).

We further examined the relationship between proliferative arrest and ferroptosis sensitivity. In HT-1080^N cells, the duration of palbociclib (2 μM) pretreatment correlated with increased RSL3 potency (Figure S2A). The concentration of palbociclib used in the pretreatment also positively correlated with RSL3 potency, and RSL3 potency was tightly correlated with the degree of proliferative arrest (Pearson $R^2 = 0.95$, $p < 0.001$) (Figure S2B and S2C). Pretreatment with the structurally distinct CDK4/6 inhibitor abemaciclib likewise reduced *E2F1* expression, decreased the percentage of cells in S phase, and sensitized

HT-1080^{N} cells to RSL3 (Figures S2D-S2F). Similar results were also obtained using doxycycline-induced overexpression of CDKN1A (Ref.[16]), which arrested cells mostly in G1, reduced *E2F1* expression, and sensitized to GPX4i treatment (Figures 1H, 1I, S2G, and S2H). Notably, CDKN1A overexpression and palbociclib treatment did not have additive effects on RSL3 sensitivity, suggesting they act through the same pathway (Figure 1H).

To further extend these results we employed complementary gain of function approaches to test whether increased cell cycle function reduced cell death sensitivity. Towards this end, we stably overexpressed the CDK4/6 partner CCND1 (cyclin D) in HT-1080^{N} cells via lentiviral transduction. CCND1 overexpression was sufficient to enhance the expression of cell cycle-associated genes (*E2F1, CCNA2*), increase the number of cells in S phase, and reduce sensitivity to RSL3 (Figure 1J-1L, and S2I). Expression of a degradation-resistant CCND1^{T286A} mutant, which accumulates to higher levels than the wild type protein,[28] did not further increase the number of S-phase cells or further reduce ferroptosis sensitivity (Figures 1J-1L, and S2I). Collectively, these results indicated that cell cycle state can alter sensitivity to GPX4i-induced ferroptosis.

Cell cycle arrest enhances sensitivity to GPX4i-induced lipid peroxidation

We hypothesized that CDK4/6 inhibition sensitized cells to GPX4i-induced ferroptosis and not a different lethal mechanism. Consistent with this hypothesis, GPX4i-induced cell death in both vehicle (DMSO)-pretreated and palbociclib-pretreated HT-1080^{N} cells was fully inhibited by the canonical small molecule ferroptosis inhibitors ferrostatin-1 and deferoxamine, but not the pan-caspase inhibitor Q-VD-OPh (Figures 2A and S3A). Thus, palbocilcib pretreatment sensitized to ferroptosis and not some other cell death mechanism.

Increased membrane lipid peroxidation is the defining feature of ferroptosis.[8,10] In HT-1080^{N} cells pretreated with palbociclib, we observed using confocal microscopy greater oxidation of the lipid peroxidation probe C11 BODIPY 581/591 (C11) in response to GPX4i treatment (Figure 2B). Doxycycline (Dox)-inducible CDKN1A overexpression in HT-1080^{N} cells likewise enhanced C11 oxidation in response to GPX4 inhibition, as detected using epifluorescent imaging (Figure S3B). We further extended these results to additional cell models, showing that 786-O renal cell carcinoma and MDA-MB-231 triple negative breast cancer cells had enhanced sensitivity to RSL3 and ML210 following palbociclib pretreatment along with increased sensitivity to C11 oxidation (Figures S3C and S3D). Thus, CDK4/6 inhibition enhanced GPX4i-induced membrane lipid peroxidation.

We initially hypothesized that enhanced lipid peroxidation and ferroptosis sensitivity were due to reduced levels of known anti-ferroptosis proteins or metabolites. However, palbociclib did not reduce the abundance of xCT (the antiporter subunit of system x_c^-), GPX4, or ferroptosis suppressor protein 1 (FSP1) protein, nor did it lower total intracellular glutathione levels (Figure 2C-2E, and S3E), eliminating several plausible sensitization mechanisms.[1] Another hypothesis was that CDK4/6 inhibition increased the susceptibility of GPX4 to inhibitor binding. We used one-dimensional SDS-PAGE to examine the apparent migration of GPX4, which is slowed by GPX4i binding.[29] Palbociclib pretreatment did not alter the apparent migration of GPX4, either when used as a single agent or in combination with a low lethal dose of RSL3, suggesting that target engagement was unaffected (Figure

2F). Thus, sensitization to membrane lipid peroxidation and ferroptosis following CDK4/6 inhibition did not appear to be explained by altered interactions between RSL3 and GPX4.

Cell cycle arrest is associated with phospholipid remodeling

We next considered whether proliferative arrest enhanced GPX4i sensitivity by altering membrane phospholipid (PL) composition. The balance between pro-ferroptotic PUFA-containing PLs and anti-ferroptotic MUFA-containing PLs is a key determinant of overall ferroptosis sensitivity[8,30]. We envisioned that increased PUFA-PL levels and/or decreased MUFA-PL levels could underlie the greater sensitivity of arrested cancer cells to GPX4i. To test this hypothesis, we compared HT-1080^{N} Control to *ACSL4* gene-disrupted ("KO") cell lines which have reduced levels of various PUFA-PLs and PUFA-containing triacylglycerols.[8,12] Consistent with our hypothesis, palbociclib pretreatment did not sensitize ACSL4$^{KO1/2}$ cells to RSL3 despite effective inhibition of Rb phosphorylation and reduced expression of *E2F1* (Figures 3A-3D). Importantly, these results also indicate that cell cycle arrest per se is insufficient to sensitize to GPX4i-induced ferroptosis in the absence of a pro-ferroptotic lipid metabolic environment.

To understand which lipids were altered by cell cycle arrest, we performed untargeted lipidomic analysis using liquid chromatography coupled to mass spectrometry (LC-MS) in Control and ACSL4$^{KO1/2}$ cells. We hypothesized that lipids altered by palbociclib in Control cells, but not ACSL4$^{KO1/2}$ cells, would be candidate regulators of ferroptosis sensitivity. Two species that changed substantially in abundance were confirmed by LC-MS/MS analysis as the PUFA-containing ether-linked phospholipids PE P-16:0/20:4 and PE P-16:0/22:6 (Figure 3E, Data S2). Interestingly, the abundances of both PE P-16:0/20:4 and PE P-16:0/22:6 were reduced following treatment with a lethal dose of RSL3 where cells were harvested just before the onset of cell death (Figure 3F). This suggested that that these two lipids could be converted to different species due to oxidation during ferroptosis.

Next, we examined whether changes observed in cultured cells in response to palbociclib were relevant in vivo. We generated HT-1080 xenograft tumors in the flanks of NOD-*scid* IL2Rgamma^{null} (NSG) mice and, once these tumors reached ~100 mm^3 in size, started treatment with palbociclib (100 mg/kg) for five days. As expected, palbociclib-treated tumors grew more slowly over the course of the experiment (Figure 3G). Moreover, in harvested tumors, we observed that palbociclib treatment significantly increased the levels of PE P-16:0/20:4 and PE P-16:0/22:6, consistent with results obtained in cultured cells (Figure 3H). We also observed an increase in the levels of the MUFA 18:1 free fatty acid, with no corresponding change in the levels of the fully saturated 18:0 precursor. These findings indicated that palbociclib treatment increased the levels of PUFA-containing PLs in cultured cells and in vivo, correlating with greater lethal lipid peroxidation and induction of ferroptosis in response to GPX4 inhibition.

Identification of cell cycle-regulated genes linked to ferroptosis

CDK4/6 regulate the transcription of hundreds of genes via the Rb-E2F pathway.[31] To identify genes that could underlie sensitization to GPX4i upon cell cycle arrest we integrated gene expression profiling with the analysis of publicly available gene expression and

compound activity datasets. Using RNA sequencing (RNA-seq) we identified 629 genes whose expression was significantly altered by palbociclib treatment (FDR $q < 0.05$) (Figure 4A and 4B, Data S3). We hypothesized that other treatments that arrest cell proliferation through distinct means might alter gene expression and enhance GPX4i sensitivity in a similar manner. The mitogen activated protein kinase (MAPK) cascade regulates cell proliferation in part by promoting expression of *CCND1*.[32] Consistent with our hypothesis, inhibition of MAPK signaling using the MAPK kinase (MEK1/2) inhibitor pimasertib (0.5 μM, 48 h) arrested cell proliferation and, like palbociclib, sensitized HT-1080^{N} cells to GPX4i treatment (Figures S4A-S4C). We therefore performed RNA-seq on pimasertib-treated cells and intersected the lists of genes whose expression was significantly altered by both palbociclib and pimasertib. The two datasets shared 498 genes, including canonical cell cycle genes (e.g., *MKI67, CCNA2,* see Data S3) that were downregulated in both conditions.[33] Next, we focused on genes whose basal mRNA expression correlated significantly with sensitivity to at least two of three GPX4i (RSL3, ML210 or ML162) tested as part of Cancer Therapeutics Response Portal database,[34] and that have likely E2F binding sites in their promoter regions based on chromatin immunoprecipitation sequencing (ChIP-seq) analysis (TargetGeneReg 2.0).[35] This integrated analysis ultimately pinpointed four genes: *MBOAT1, GPD2, EMP2*, and *MYO19* (Figures 4A-4C).

MBOAT1 (membrane bound O-acyltransferase domain containing 1) is a MUFA-specific lysophospholipid acyltransferase (LPLAT) recently linked to ferroptosis regulation.[36,37] Less oxidizable MUFAs can suppress ferroptosis by displacing more oxidizable PUFA species from plasma membrane phospholipids.[8,38,39] Lower *MBOAT1* expression upon cell cycle arrest could sensitize to GPX4i by reducing the levels of anti-ferroptotic MUFA-PLs[8,37,40] and/or allowing for increased levels of PUFA-PLs, consistent with our lipidomic results (Figure 3). GPD2 (glycerol-3-phosphate dehydrogenase 2) is a mitochondrial enzyme that helps generate reduced Coenzyme Q10 (CoQ10), a ferroptosis inhibitory metabolite.[41] Downregulation of *GPD2* may explain sensitization to GPX4i. Connections between EMP2 (epithelial membrane protein 2) or MYO19 (myosin XIX) and ferroptosis were less obvious. However, reciprocal analysis of the CTRP dataset revealed that basal *EMP2* expression was among the strongest correlates of sensitivity to GPX4i across the entire transcriptome (Figure 4D).

We sought independent evidence that these four genes were likely to be cell cycle regulated. First, we examined data from TCGA, specifically looking at the correlation between *RB* mutation status and expression of all four candidate genes. Since our analysis had mainly employed fibrosarcoma cells, we focused on the sarcoma (SARC) patient cohort. Our hypothesis was that *RB* mutation should be associated with increased expression of all four target genes (i.e., mimicking the effect of constitutive CDK4/6 activity). Generally consistent with this hypothesis, *RB* mutation was significantly (Student's t-test, $p < 0.05$) associated with higher expression of *GPD2, EMP2* and *MYO19*, while no significant association was observed for *MBOAT1* (Figures S4D). Next, from a database of transcriptomic profiles acquired at various points across the cell cycle of cultured HeLa cells[42] we looked for functional evidence of periodic gene expression across the cell cycle. Data were available for *MBOAT1* and *GPD2*. In this analysis, *MBOAT1* expression peaked at the G1/S transition (periodic rank: 178), similar to *E2F1* (periodic rank: 134), while

GPD2 expression was more dispersed across the cell cycle (periodic rank: 1,501). No data were available for *EMP2* or *MYO19*. However, EMP2 overexpression can arrest lung cancer cells in G1, consistent with a link to cell cycle regulation.[43]

To investigate further, we performed targeted gene expression analysis in HT-1080^{N} cells. All four candidate genes were downregulated in HT-1080^{N} cells treated with nutlin-3 and/or palbociclib treatment, with *MBOAT1* and *EMP2* showing the strongest downregulation in cultured HT-1080 cells (Figure 4E). Strong transcriptional downregulation of *MBOAT1* and *EMP2*, but not *GPD2* or *MYO19*, was also observed in HT-1080 xenograft tumors treated with palbociclib (Figure 4F). Transcription of the closely related genes *MBOAT2* (to *MBOAT1*) and *EMP3* (to *EMP2*) were not decreased by palbociclib treatment (Figure 4F). Unfortunately, we were unable to examine effects at the protein level as we could not identify antibodies that detected endogenous MBOAT1 or EMP2 protein, a limitation of this study. Nonetheless, based on these results, we focused further on *MBOAT1* and *EMP2* as candidate cell cycle-dependent regulators of ferroptosis.

MBOAT1 can regulate ferroptosis sensitivity

MBOAT1 uses oleoyl-CoA (a MUFA) as a substrate to synthesize MUFA-PLs (Figure 5A).[36,37,44] MBOAT1 is one of four mammalian MBOAT-family lysophospholipid acyltransferases (MBOAT1, MBOAT2, MBOAT5/LPCAT3, and MBOAT7), each with partially distinct substrate specificities.[45] Consistent with the hypothesis that *MBOAT1* gene expression is cell cycle-regulated, nutlin-3 reduced *MBOAT1* expression in a p53-dependent manner while palbociclib and pimasertib reduced *MBOAT1* expression in both HT-1080 Control and p53^{KO} cells (Figure 5B). *MBOAT2, MBOAT5/LPCAT3*, and *MBOAT7* are all classified as non-periodic genes in Cyclebase.[42] Indeed, Dox-induced CDKN1A overexpression in HT-1080 cells reduced the expression of *MBOAT1* but not *MBOAT2* or *MBOAT5* (Figure 5C), and palbociclib treatment reduced *MBOAT1* expression in cultured A375^{N} (p53 wild type), T98G^{N} (p53 mutant), and H1299^{N} (p53 null) cells while *MBOAT2* and/or *MBOAT5* expression was not reduced (Figure 5D). Thus, various cell cycle arresting conditions resulted in selective downregulation of *MBOAT1* expression.

To test whether reduced *MBOAT1* expression was necessary for enhanced sensitivity to GPX4i upon cell cycle arrest, we engineered HT-1080 cell lines where epitope (FLAG)-tagged wild type MBOAT1 (MBOAT^{WT}) or a predicted catalytic-dead MBOAT1^{H381A} mutant[46] were expressed under Dox-inducible control (Figure 5E). Dox-induced overexpression of MBOAT^{WT} abrogated palbociclib-mediated sensitization to RSL3 (Figure 5F). By contrast, overexpression of MBOAT1^{H381A} exacerbated the lethality of RSL3, possibly due to a dominant negative effect (Figure 5F). Similar results were obtained when using pimasertib pretreatment instead of palbociclib pretreatment, demonstrating that these effects were not limited to direct CDK4/6 inhibition (Figure 5G). Importantly, MBOAT1^{WT} overexpression did not prevent palbociclib from reducing Rb phosphorylation, lowering *E2F1* expression, or arresting cell cycle progression (Figures S5A-C). Collectively, these results demonstrated that *MBOAT1* overexpression was sufficient to revert sensitization to GPX4i upon cell cycle arrest.

We hypothesized that MBOAT1 expression suppressed ferroptosis by altering lipid metabolism. Supporting this hypothesis, Dox-inducible overexpression of MBOAT1^{WT} but not MBOAT1^{H381A} reduced the levels of PE P-16:0/20:4 and prevented the accumulation of PE P-16:0/20:4 upon palbociclib treatment (Figure 5H). By contrast, the basal level of FA 18:1 (oleic acid) was decreased by MBOAT1^{WT} expression and was only partially recovered by palbociclib treatment. A different MUFA species, PE *a*-16:1/18:1, where '*a*' denotes that this alkyl lipid may be either an ether lipid or plasmalogen, was largely unaffected by palbociclib treatment but substantially increased by MBOAT1^{WT} expression (Figure 5F). By contrast, Dox-induced MBOAT1^{H381A} expression did not result in similar changes in the abundance of these PUFA and MUFA species (Figure S5D). Thus, MBOAT1 may suppress GPX4i sensitivity by reducing PUFA-PL levels and/or increasing MUFA-PL levels.[37]

We next investigated whether *MBOAT1* loss of function alone was sufficient to enhance ferroptosis sensitivity in asynchronously cycling cells and obtained several lines of evidence that this was not the case. First, a clonal *MBOAT1* gene disrupted human HAP1 haploid cell line did not show altered RSL3 sensitivity following palbociclib pretreatment (Figure 5I). Of note, palbociclib-treated HAP1 MBOAT1^{KO} cells displayed a greater propensity to arrest in the G2/M phase than palbociclib-treated wild type cells, consistent with some role for MBOAT1 in progression through the cell cycle, but this phenotype was not examined further here (Figure 5J). Second, three independent clonal HT-1080^{N} *MBOAT1* gene-disrupted cell lines exhibited no difference in RSL3 sensitivity compared to an unmodified Control cell line (Figure S5E). Third, a short interfering RNA (siRNA) targeting *MBOAT1* did not alter ferroptosis sensitivity in T98G^{N} or A375^{N} cell lines (Figures S5F-S5I). Collectively, these findings indicated that *MBOAT1* downregulation may be necessary for sensitization to GPX4i upon CDK4/6 inhibition but that *MBOAT1* downregulation alone was insufficient to enhance GPX4i sensitivity in normally cycling cells.

EMP2 downregulation sensitizes to ferroptosis

We next turned our attention to *EMP2*. Low basal *EMP2* expression was highly correlated to all three GPX4i in the CTRP (Figure 4D). *EMP2* was also significantly downregulated in response to palbociclib in both cultured cells and tumor xenografts (Figures 4E and 4F). EMP2 is one of four related peripheral myelin protein 22-family tetraspanins: PMP22, EMP1, EMP2, and EMP3.[47] In HT-1080^{N} cells, palbociclib and abemaciclib both reduced *EMP2* expression with little effect on the expression of *PMP22* or *EMP3*, and a weaker downregulation of *EMP1* (Figure 6A). Dox-inducible CDKN1A overexpression in HT-1080^{N} cells strongly reduced *EMP2* expression, and the effect of palbociclib was not additive with CDKN1A overexpression, consistent with a single pathway (Figure 6B). *EMP2* expression was also substantially downregulated in other p53 wildtype cells (Caki-1^{N}, A375^{N}) upon treatment with nutlin-3 or pimasertib (Figure S6A). Collectively, these findings were consistent with *EMP2* downregulation upon cell cycle arrest.

We examined whether loss of *EMP2* function alone was sufficient to regulate ferroptosis sensitivity. Notably, in HT-1080^{N} cells genetic silencing of *EMP2* alone using two different siRNAs was sufficient to sensitize to RSL3-induced ferroptosis, almost to the level of palbociclib alone (Figures 6C-E). This sensitization was due to the induction of ferroptosis,

as it was fully suppressed by ferrostatin-1 (Figure 6E). Similar results were obtained using these siRNAs in Caki-1 cells (Figures S6B and S6C).

We next isolated a clonal HT-1080^{N} *EMP2* gene-disrupted cell line (EMP2^{KO}) and a matched Control cell line that had undergone the CRISPR process without modification. Using genomic DNA sequencing, we confirmed that EMP2^{KO} cells contained an early stop codon (see Methods). Moreover, by RT-qPCR analysis we detected reduced *EMP2* expression in the gene-disrupted cell line and no change in the expression of *EMP3* (Figure S6D). Both the Control and EMP2^{KO} cell lines were sensitive to the effects of palbociclib, exhibiting equivalent reductions in the mRNA levels of the cell cycle genes *E2F1* and *CCNA2* (Figure S6E), and both cell lines arrested in G1 after palbociclib treatment (Figure S6F), indicating that *EMP2* disruption per se did not alter the cell cycle or the ability of CDK4/6 inhibition to arrest cell cycle progression. *EMP2* disruption also did not alter *MBOAT1* transcript levels (Figure S6G).

We then examined cell death in Control and EMP2^{KO} cells. Compared to the Control cell line, EMP2^{KO} cells were basally sensitized to the GPX4i RSL3 and ML210, slightly sensitized to erastin2, and not sensitized to the pro-apoptotic agent bortezomib (Figure S6H). Consistent with results obtained using siRNA treatment, palbociclib treatment and genetic disruption of *EMP2* each sensitized to RSL3 treatment to an equivalent extent, and these effects were not additive, implying action through a common mechanism (Figure 6F). By contrast, palbociclib pretreatment and *EMP2* disruption or silencing weakly affected sensitivity to erastin2 in HT-1080^{N} or Caki-1^{N} cells (Figure S6I-J). Together these results indicated that loss of *EMP2* expression was sufficient to sensitize to ferroptosis triggered by direct GPX4 inhibition.

Loss of *EMP2* promotes PUFA enrichment in phospholipids

Palbociclib treatment causes the accumulation of PUFA-PEs in vitro and in vivo (Figures 4E, and 4H). We hypothesized that loss of *EMP2* may sensitize to ferroptosis by promoting the accumulation of PUFA-PEs. Using untargeted LC-MS/MS, we detected 678 lipid species with high confidence in Control and EMP2^{KO} cells treated with DMSO or palbociclib (Figure S7A). Given that loss of *EMP2* is sufficient to promote GPX4i sensitization, and that functional *EMP2* is necessary for palbociclib to sensitize to GPX4i (Figure 6F), we designed a strategy to filter our initial list to focus on lipids that may be relevant for this phenotype (Figure S7A and Methods). While saturated fatty acid (SFA), MUFA, and PUFA-containing species were broadly increased by palbociclib treatment and *EMP2* gene disruption, the plurality of PUFA-containing species that were increased belonged to the plasmalogen-PE (PE P) class (Figure S7B). Furthermore, every PE P and PE lipid that was significantly altered contained a PUFA tail group (Figure S7B).

To analyze the dataset more broadly, we performed Bioinformatics Methodology for Pathway Analysis (BioPAN)[48] on the lipidomics dataset. BioPAN revealed similarities between the pathways altered by palbociclib in Control cells, and pathways altered by EMP2^{KO} cells compared to Control (Figure S7C). Synthesis of PE phospholipids from PS lipids was enriched in both conditions, while catabolism of PE to PS was disenriched. Synthesis of PE P lipids was highly enriched (z-score > 4) in both ferroptosis-sensitizing

conditions (Figure S7C). Next, we performed principal component analysis (PCA) and found that the Control + palbociclib and EMP2^{KO} + DMSO conditions clustered closely together (Figure 6G). Specifically, these conditions were primarily separated from the Control + DMSO samples in principle component 1 (Figure 6G). Further analysis of the PCA loadings plots revealed that compared to phosphatidylcholines, which were dispersed across principal component 1, PE and PE P lipids appeared to contribute to an increase in principal component 1 (Figure 6H).

We therefore more closely investigated the specific PE and PE P lipids altered by palbociclib treatment and EMP2^{KO} (Figures S7A and S7B). The only PE lipid that met the statistical criteria was PE 16:0_20:4 (Data S4). Of the six PE P lipids significantly altered, a plurality (3 of 6) contained a 20:4 tail group: PE P-16:0_20:4, PE P-18:0_20:4, and PE P-22:0_20:4 (Data S4). All four 20:4-containing PE and PE P lipids were increased to the same extent in the Control + Palbociclib, EMP2^{KO} + DMSO, and EMP2^{KO} + palbociclib conditions compared to the Control + DMSO condition (Figure 6I and 6J). Thus, both palbociclib treatment and EMP2^{KO} enrich for pro-ferroptotic 20:4 tail groups in PE and PE P phospholipids, consistent with a lipid-dependent mechanism of ferroptosis sensitization.

CDK4/6 inhibition and GPX4 inhibition enhance lipid peroxidation in vivo

Existing covalent GPX4 inhibitors such as RSL3 are unsuitable for use in vivo due to poor bioavailability. From the patent literature, we identified a candidate orally bioavailable GPX4 inhibitor, compound 28 (Figure 7A).[49] We confirmed that compound 28 potently induced cell death in cultured HT-1080^{N} cells and that this lethality was enhanced by palbociclib pretreatment (Figure 7B). Cell death induced by compound 28 was suppressed by co-treatment with ferrostatin-1, consistent with the induction of ferroptosis (Figure 7C).

Both palbociclib and compound 28 independently have the potential to cause significant on-target toxicities in animals (e.g., kidney damage upon *Gpx4* disruption).[50] We developed a staggered oral dosing schedule for both agents that replicated the palbociclib pretreatment approach used in cultured cells (Figure 7D). This dosing schedule was generally tolerated by mice over 17 days, albeit with a degree of weight loss (Figures 7E). Only mice treated with the combination of palbociclib and compound 28 had reduced tumor sizes at the experimental endpoint relative to untreated controls (Figure 7F). Compound 28 appeared to engage GPX4 effectively in the xenografts, both alone and in the combination, as judged by slower apparent GPX4 migration (Figure 7G). Tumors extracted from mice that received the combination treatment also showed significantly lower levels of PE P-16:0/20:4 and PE P-16:0/22:6 (Figure 7H). Analysis of staining for 4-hydroxynonenal, a breakdown product of lipid peroxidation, showed significantly higher levels of this marker in xenografts from animals that received both palbociclib and compound 28 than xenografts exposed to either compound alone (Figure 7I). Thus, the combination of a CDK4/6 inhibitor and GPX4i may induce more lipid peroxidation in tumor cells in vivo than either compound alone.

DISCUSSION

p53 is reported to induce, suppress, or have no effect on ferroptosis.[13,14,16,17,51] We find that wild type p53 stabilization can reduce sensitivity to ferroptosis triggered by

system x_c^- inhibition yet sensitize to ferroptosis triggered by direct GPX4 inhibition. This is a striking example of the context-dependent nature of ferroptosis regulation.[11] Mechanistically, changes in the lipidome that favor lipid peroxidation appears to offer the best explanation for sensitization to GPX4i. If so, why do these changes not also sensitize to system x_c^- inhibitors? One possibility is that the composition of the lipidome does not matter until GPX4 is fully inactivated, which occurs more slowly in p53-stabilized cells deprived of cystine due to reduced consumption of glutathione.[16,17] Alternatively or in parallel, certain *MBOAT1*-and/or-*EMP2*-regulated lipids may be more important for the execution of ferroptosis in response to direct GPX4 than system x_c^- inhibition.[12] Comparing the lipidome of cells treated with system x_c^- inhibitors versus direct GPX4 inhibitors should help resolve this issue.

We identify diverse genetic and pharmacological interventions that arrest cell cycle progression and sensitize to GPX4 inhibitors, at least in the cells examined here. Interestingly, cancer persister cells that tolerate chemotherapy are hypersensitive to GPX4 inhibitors.[52,53] Our results and other studies[54] suggest that therapy-induced cell cycle arrest could help sensitize to GPX4 inhibition by modulating membrane phospholipid composition. Indeed, persister cells that continue to transit through the cell cycle are less sensitive to GPX4 inhibitors than non-cycling persister cells.[55] Cell cycle arrest is generally thought to render cells more resistant to cell death but it seems that this may not be true for ferroptosis.

Our RNA Seq analysis, together with consideration of the CTRP database, pinpointed *MBOAT1* and *EMP2* as candidate regulators of ferroptosis sensitivity. In line with recent findings,[37] we show that overexpression of MBOAT1 can inhibit ferroptosis in response to GPX4 inhibitors, plausibly by increasing the incorporation of MUFAs instead of PUFAs into membrane phospholipids.[7,56] We show that loss of *EMP2* expression is sufficient to increase the levels of PUFA-PL species that are linked to the induction of ferroptosis. We cannot exclude the possibility that lipid species not detected in our analysis explain the modulation of ferroptosis sensitivity. However, an increased PE-PUFA/MUFA ratio provides a plausible explanation for GPX4i hypersensitivity.[30] While we have generalized our findings to cell lines from three different lineages (sarcoma, renal cell carcinoma, melanoma) the limits of our model in other cancers remain to be fully defined. For example, breast cancer cells treated with palbociclib do not appear to downregulate *MBOAT1* or *EMP2*,[57] and therefore may not be sensitized to ferroptosis.

Our results pinpoint loss of *EMP2* as a sufficient sensitizer to GPX4i treatment, at least in the cells examined here. How EMP2 expression alters membrane phospholipid composition will require further elucidation but could involve interactions with plasma membrane-localized lipid remodeling enzymes or effects on lipid trafficking. Another family member, EMP1, can promote ferroptosis in some cells[58]. This raises the possibility that EMP1 and EMP2 are mutually antagonistic with respect to ferroptosis regulation. Anti-EMP2 inhibitory antibodies have been shown to control tumor xenograft growth,[59,60]. It may be interesting in the future to examine combinations of these agents with GPX4i for cancer therapy.

We explored the potential for combining GPX4 inhibition with other treatments in vivo. We used a clinical-candidate GPX4 inhibitor (compound 28) reported in the patent literature. Compound 28 only had a significant effect on HT-1080 xenografts tumor volume when combined with palbociclib administration. Moreover, palbociclib enhanced the levels of lipid peroxidation induced by compound 28. Another GPX4 inhibitor, compound 24, was also recently described.[29] Compound 24 was tolerated by mice but had little effect alone on the growth of a diffuse large B cell lymphoma xenograft. It may be that GPX4 inhibition alone is not sufficient in many cases to affect tumor growth. Notably, compound 28 delivered via oral gavage appears able to engage GPX4 in tumor xenografts, a potential advantage over compound 24 and other GPX4 inhibitors not suitable for oral administration.[19] Toxicity is a concern with all GPX4 inhibitors[50] and we did observe body weight loss in mice treated with compound 28, even when using a schedule that saw only two doses a week. This toxicity will have to be carefully monitored in future studies. However, the existence of compound 28 opens a path to these and other new investigations of ferroptosis in vivo.

Limitations of the study

We examined the effect of stabilizing wild type p53, in cancer cells, in culture, for 48 h before the initiation of ferroptosis, using direct pharmacological inhibitors of system x_c^- or GPX4. Our findings may only be applicable to these settings and explain in part why studies that induce ferroptosis with different reagents yield distinct results.[18,51] *MBOAT1* genetic perturbation is insufficient to sensitize to GPX4i alone, possibly due to redundancy with *MBOAT2*.[37] The correlation between *EMP2* gene expression and ferroptosis sensitivity is strong. However, we have not been able to study EMP2 protein due to a lack of suitable reagents. Also, the mechanism linking *EMP2* expression to changes in lipid metabolism remains to be defined. In vivo combination studies are challenging when using drugs that have potential dose-limiting toxicities. Our compound 28 dosing strategy may only be effective in the context studied here and require further optimization for different cell models and drug combinations.

SIGNIFICANCE

It may be possible to target the ferroptosis mechanism to treat cancer and other diseases. Emerging evidence indicates that system x_c^- inhibition and direct inhibition of GPX4 do not induce ferroptosis in the same manner. Here, we show that stabilization of p53 and inhibition of CDK activity create unique cell states that exhibit distinct responses to cystine deprivation versus direct GPX4 inhibition. We show that cell cycle arrest is associated with transcriptional downregulation of several genes, including *MBOAT1* and *EMP2*, which can regulate the abundance of ferroptosis-associated lipids and thereby alter sensitivity to GPX4 inhibition. Using an orally bioavailable GPX4 inhibitor we also showed that combined CDK4/6 and GPX4 inhibition can enhance lipid peroxidation in tumors in vivo. These developments could help open new avenues to investigate ferroptosis in vivo.

STAR METHODS

RESOURCE AVAILABILITY

Lead Contact—Further information and requests for resources and reagents should be directed to and will be fulfilled by the Lead Contact, Scott Dixon (sjdixon@stanford.edu).

Materials Availability—Plasmids, cell lines and other materials generated in this study will be shared by the lead contact upon request.

Data and Code Availability

- Underlying deviation scores for the nutlin-3 modulatory screen is available in Data S1. Processed data for lipidomics experiments are available in Data S2 and Data S4. RNA-seq data have been deposited at GEO (GSE180265) and are publicly available as of the date of publication. Summarized RNA-seq data are available in Data S3. Data S1-S4 and uncropped immunoblots are available online at the Mendeley Data Repository and are available at the date of publication. The DOI is listed in the key resources table.
- One script used to quantify 4-HNE staining have been deposited at the Mendeley Data Repository and are publicly available as of the date of publication. The DOI is listed in the key resources table.
- Any additional information required to reanalyze the data reported in this paper is available from the lead contact upon request.

EXPERIMENTAL MODELS AND STUDY PARTICIPANT DETAILS

Cell lines.—HT-1080^{N} (M), Caki-1^{N} (M), H1299^{N} (M), T98G^{N} (M), and A375^{N} (F) cells were described previously.[16,22,61] Sex of cell lines is indicated in parentheses. HT-1080^{N} Control and gene-disrupted p53^{KO} cells were described previously.[16] HT-1080^{N} rtTA-CDKN1A cell lines were described.[17] HT-1080^{N} Control and ACSL4$^{KO1/2}$ cell lines were described previously.[12] H460 (M) Control and gene disrupted FSP1^{KO} cell lines were described previously.[62] A HAP1 (M) *MBOAT1* gene-disrupted cell line and a paired wild type control cell line were purchased from Horizon Discovery (Cambridge, UK). 786-O (M) and MDA-MB-231 (F) cells were obtained from ATCC (Manassas, VA). The generation of HT-1080^{N} HA-CCND1^{WT} and HT-1080^{N} HA-CCND1^{T286A}, HT-1080^{N} rtTA-MBOAT1^{WT} and HT-1080^{N} rtTA-MBOAT1^{H381A}, and HT-1080^{N} Control and EMP2^{KO} cells are described below. All HT-1080-based cell lines were cultured in DMEM Hi-glucose medium (Cat# MT-10-013-CV, Corning Life Science, Corning, NY) supplemented with 10% fetal bovine serum (FBS, Cat# 26140-079, Gibco/Thermo Fisher Scientific), 1% non-essential amino acids (NEAAs) (Cat# 11140-050, Life Technologies, Carlsbad, CA), and penicillin + streptomycin (P/S) (5000 U/mL) at 1x concentration (Cat# 15070-063, Life Technologies). H460, HAP1^{N}, T98G^{N}, H1299^{N}, 786-0 and MDA-MB-231 cells were grown in DMEM Hi-glucose medium supplemented with 10% FBS and 1x P/S. A375^{N} and Caki-1^{N} cells were cultured in McCoy's 5A media (Cat# MT-10-050-CV, Corning Life Science) supplemented with 10% FBS and 1x P/S. All cells were grown in humidified incubators (Thermo Fisher Scientific) at 37°C with 5% CO2.

METHODS DETAILS

Chemicals and reagents.—ML162 was synthesized by Acme (Palo Alto, CA). Erastin2 (Cat# 27087) and deferoxamine (Cat# 14595) were obtained from Cayman Chemicals (Ann Arbor, MI). Palbociclib (Cat# S1116), pimasertib (Cat# S1475), and 1*S*,3*R*-RSL3 (simply, RSL3) (Cat# S8155) were obtained from Selleck Chemicals (Houston, TX). Doxycycline (Dox) (Cat# D3447), ML210 (Cat# SML0521), ferrostatin-1 (Cat# SML0583) and propidium iodide (Cat# P4170) were obtained from Sigma-Aldrich (St. Louis, MO). Abemaciclib (Cat# HY-16297A) was obtained from MedChem Express (Princeton, NJ). Bortezomib (Cat# NC0587961), Q-VD-OPh (Cat# OPH00101M), etoposide (Cat# 12-261-00), DAPI (Cat# D1306) and C11 BODIPY 581/591 were from Thermo Fisher Scientific (Waltham, MA). Compound 28 was synthesized as described[49] and provided as a gift by P. Beltran (Ferro Inc). Dox was dissolved in deionized water and stored at −20°C. C11 BODIPY 581/591 was dissolved into methanol and stored at −20°C. All other compounds were dissolved in dimethyl sulfoxide (DMSO) and then stored at −20°C. The compound library (Cat# L1700) was obtained from Selleck Chemicals.[8]

Cell death measurement.—Cells were seeded to obtain 70-80% confluency at the time of lethal stimulus addition. All HT-1080-based cell lines and Caki-1^{N} cells were seeded at 1,500 cells/well in DMSO treatment and at 3,000 cells/well in 96-well plates for treatment with nutlin-3, palbociclib, pimasertib, or abemaciclib. A375^{N} cells were seeded at 3,000 cells/well for DMSO conditions and at 6,000 cells/well in 96-well plates for nutlin-3 and palbociclib treatment conditions. HAP1^{N} parental and MBOAT1^{KO} cells were seeded at 2,500 cells/well for DMSO conditions and 5,000 cells/well in 96-well plates for palbociclib treatment. HT-1080^{N} rtTA-CDKN1A cells were seeded at 1,500 cells/well for DMSO treatment, and 3,000 cells/well in 96-well plates for palbociclib, Dox, and Dox + palbociclib treatment. HT-1080^{N} rtTA-MBOAT1^{WT} and HT-1080^{N} rtTA-MBOAT1^{H381A} cells were seeded at 1,500 cells/well for DMSO and Dox treatment, and 3,000 cells/well in 96-well plates for palbociclib and Dox + palbociclib treatment. The next day, cells were treated with the indicated pretreatment. For these cell lines, the concentrations of treatment compounds were as follows: palbociclib (2 μM), nutlin-3 (10 μM), abemaciclib (1 μM), pimasertib (0.5 μM), Dox (0.1 μg/mL). 48 h after pretreatment was initiated, cells were exposed to a lethal stimulus (e.g., RSL3). Additionally, SYTOX Green (20 nM, Cat# S7020, Life Technologies/Thermo Fischer Scientific) was added to the growth medium to track cell death. Images were acquired using either an IncuCyte ZOOM imaging system (Model 4459, Essen BioSciences, Ann Arbor, USA) or an IncuCyte S3 live cell analysis instrument (Sartorius, Göttingen, Germany) housed within a tissue culture incubator maintained at 37°C with 5% CO_2. In each well, phase contrast, red (excitation: 585 ± 20, emission: 665 ± 40, acquisition time: 800 ms), and green (excitation: 460 ± 20, emission: 524 ± 20, acquisition time: 400 ms) images were obtained at 10x magnification. The images were analyzed using either the ZOOM software package (V2016A/B) or the S3 software package. Lethal fraction was calculated as described.[63]

Cell death studies of 786-O and MDA-MB-231 cells were conducted as follows. Cells were seeded in 10 cm plates at the density of 800,000 cells/plate and treated with vehicle control or palbociclib (1 μM) for 48 h. After pretreatment, cells were trypsinized, seeded

into 12-well plates (80,000 cells per well), and treated with ferroptosis-inducing compounds. At the end of treatment, the culture medium was collected. Cells were then washed with 300 μL PBS and the PBS was combined with culture medium. Cells were then trypsinized using 100 μL trypsin and neutralized with the collected culture medium. After centrifugation at 500 x *g* for 5 min, cells were resuspended in 180 μL PBS containing 2 μg/mL propidium iodide (PI) and PI-positive dead cells were detected by flow cytometry using a BD fortessa X-20 cytometer. Percent cell death was determined as the percentage of PI-positive cells in the sampled population.

Small molecule modulation screen.—HT-1080^{N} cells were seeded into 384-well plates at a density of 1,000 cells per well. The next day, either DMSO or nutlin-3 (final concentration: 10 μM) was added to the growth media. 48 h after the addition of DMSO or nutlin-3, a library of 261 bioactive compounds was added to each plate (final concentration: 5 μM) using a Versette automated liquid handler as described.[8] Images were acquired every 4 h using the IncuCyte ZOOM as described above. Lethal fraction scores for each time point were calculated as above, using custom Python code. Area-under-curve (AUC) analysis was performed in Python measuring the AUC of the lethal fraction versus time. AUC values were normalized to the total time of the experiment (nAUC). For each bioactive compound, the nAUC of each test compound alone was compared to the nAUC of nutlin-3 alone, as well as the nutlin-3 + compound condition. Compound-compound interactions were assessed using the Bliss Independence model, yielding an interaction score for each compound. Z-scores were computed across the set of all compound interaction scores and plotted.

Cloning for MBOAT1 overexpression.—The coding sequence (CDS) of *MBOAT1* (NM_001080480.3) was obtained from NCBI. A gene block was designed such that the CDS was flanked on either side by overhangs useful for subsequent cloning. At the 5’ end, a Kozak consensus sequence was inserted immediately prior to a sequence encoding a 1x FLAG tag and a 15-nucleotide spacer (5’-ACTAGTCCAGTGTGGTGGAATTCTGCAGATACCATGGATTACAAGGATGACGACG ATAAGGCCCGGGCGGATCCC-3’). The 3’ overhang sequence was as follows (5’-ATCCAGCACAGTGGCGGCCGCTCGACAATC-3’). The final sequence (hereafter denoted “MBOAT1 insert”) was confirmed by Sanger sequencing. The destination plasmid pLenti TRE3G Dest (pSD292) was a generous gift of Jan Carette (Stanford School of Medicine). pSD292 was linearized by digestion with *EcoRV* (Cat# R3195S, New England Biolabs, Ipswich, MA) as per manufacturer protocol. The MBOAT1 insert was cloned into pSD292 through a Gibson assembly protocol wherein 100 ng of linearized pSD292 (19.9 fmol) and a 3x molar ratio of insert (59.7 fmol) were combined with the Gibson assembly mix (Cat# E5510S, New England Biolabs) per manufacturer instructions. The new plasmid, termed “pLenti TRE3G-MBOAT1”, was transformed into NEB 5-alpha competent *E. coli* provided with the Gibson assembly kit (Cat# E5510S, New England Biolabs) per manufacturer protocol. pLenti TRE3G-MBOAT1^{H381A} was generated by using the Q5 mutagenesis kit (Cat# E0554S, New England Biolabs). In brief, forward (5’-TGCTTTGTGGgcTGGTGTCTAC-3’) and reverse (5’-GACAGGATGAAGGTTAGC-3’) primers were added to the master mix at 10 μM each. The annealing temperature was 56°C.

All other steps were performed per manufacturer instructions. pLenti TRE3G-MBOAT1^{H381A} was transformed into NEB 5-alpha competent *E. coli* as above.

Lentivirus production.—293T cells were seeded in 6-well plates (Cat# 3516, Corning) at a density of 500,000 cells/well. The next day, medium was removed and replaced with DMEM lacking P/S. Cells were transfected using 1,000 ng of plasmid DNA for pLenti TRE3G-MBOAT1 or pLenti TRE3G-MBOAT1^{H381A}, together with the lentiviral packaging plasmids pMD2.G (250 ng, Cat# 12259, Addgene, Watertown, MA) and psPax2 (750 ng, Cat# 12260, Addgene) using Lipofectamine LTX transfection reagents (Cat# 15338-100, Life Technologies) diluted in OptiMEM media (Cat# 31985070, Thermo Fisher Scientific) to a final volume of 250 μL. The transfection mixture was incubated for 15 min and then added dropwise to the cells. The cells were then incubated overnight. The next day, virus-containing medium was collected from both plates and replaced with 2 mL of fresh medium. 8 h later, the medium was collected and replaced with 2 mL fresh medium. The following morning, the medium was collected a final time (for a total of 6 mL virus-containing medium per virus). The viral media was filtered using a 0.45 μm filter (Cat# SLHV033RS, Millex/Sigma Aldrich, St. Louis, MO), aliquoted, and frozen at −80°C until use.

Generation of CCND1-overexpressing cells.—Lentiviruses that express the vector for HA-CCND1$^{WT/T286A}$ were described.[28] HT-1080^{N} cells were seeded in a 6-well dish such that each well contained 50,000 cells (day 0). On day 1, cells were treated with lentivirus-containing growth medium containing 8 μg/mL polybrene at a viral MOI of 1. On day 2, medium was removed, and puromycin was added in fresh growth medium at a final concentration of 1 μg/mL. On day 4, medium was replaced with fresh medium lacking puromycin, and the surviving cells were used in subsequent experiments.

Generation of MBOAT1-overexpressing cells.—HT-1080^{N} rtTA cells,[17] were seeded at 3,000 cells/well in 96-well plates (Cat# 781660, BrandTech, Essex, CT). The next day, cells were infected with a serial dilution of either MBOAT1^{WT} or MBOAT1^{H381A} lentiviral particles in growth media containing 8 μg/mL polybrene (Cat# H9268-5G, Sigma Aldrich). 24 h later, viral media were removed and replaced with media containing 1 μg/mL puromycin (Cat# A11138-03, Thermo Fisher Scientific). Cells infected with 10% virus-containing media completely survived puromycin selection. Therefore, HT-1080^{N} rtTA cells were infected using 10%/90% virus-containing medium/regular growth medium containing 8 μg/mL polybrene. 24 h later, viral medium was removed, 1 μg/mL puromycin was added for 48 h to eliminate uninfected cells. The cell lines were expanded into cultures referred to as HT-1080^{N} rtTA-MBOAT1^{WT} and HT-1080^{N} rtTA-MBOAT1^{H381A}.

Isolation of MBOAT1^{KO} and EMP2^{KO} cell lines.—pSpCas9(BB)-2A-GFP plasmid was obtained from Addgene (Cat# 48138). sgRNA primers for *MBOAT1* were designed as follows. The forward primer for the sgRNA was 5’-CACCGGGACTACATAGCCTTCATTG and the reverse primer was 5’-AAACCAATGAAGGCTATGTAGTCCC. sgRNA primers for *EMP2* were synthesized as follows. The forward primer for the sgRNA was 5’-GAAACTTACATTGTCGACGG and the reverse primer was 5’-CCGTCGACAATGTAAGTTTC. 5’ and 3’ adaptors were added to the primers

to match the *Bsp*I cleavage sites of pSpCas9(BB)-2A-GFP such that the final primers were F: 5' CACCGGAAACTTACATTGTCGACGG and R: 5'-AACCCGTCGACAATGTAAGTTTCC. In both cases, primers were diluted to a final concentration of 10 μM in 10 μL of H_2O and then heated to 95°C, cooled to 25°C at a rate of 2.5°C/min. The duplexed oligo was diluted 1:200 in H_2O and then ligated into the backbone through the following reaction. 100 ng backbone, 2 μL of the diluted oligo duplex, 2 μL of 10x FastDigest buffer (Thermo Fisher Scientific), 1 μL 10 mM DTT, 1 μL 10 mM ATP, 1 μL FastDigest *Bpi*I (Cat# D1014, Thermo Fisher Scientific), 0.5 μL T4 DNA ligase (Cat# EL0014, Thermo Fisher Scientific), and up to 20 μL of H_2O were combined. The mixture was incubated for six cycles of 37°C, 5 min then 21°C, 5 min. The product was transformed into competent DH5α cells as above, and purified plasmid was collected from the cells using the Qiagen Plasmid Plus Midi Kit (Cat# 12943) per manufacturer protocol.

For both genes, HT-1080^{N} cells were transfected with 1 μg of plasmid using Lipofectamine LTX reagent as described above. Briefly, 50,000 cells were seeded into a well of a 6-well plate. Cells were transfected, and then transfection media was removed the following morning. 24 h later, cells were trypsinized and sorted at the Stanford FACS facility. GFP+ cells were sorted into a 96 well plate containing 200 μL of media that contained 30% FBS such that only one cell was deposited into each well. Homogenous populations were allowed to grow for three weeks, and then each clone was expanded and the *MBOAT1* or *EMP2* genomic loci were sequenced. Specifically, genomic DNA was purified using NucleoSpin® Tissue DNA isolation kits (Cat# 740952.50, Takara Bio, Otsu, Shiga, Japan). The genomic loci were amplified by PCR using sequencing primers in Table S1, and then sequenced at Sequetech Corporation. For *MBOAT1*, one unmodified Control and three gene-disrupted ("KO") cell lines were isolated. Two clones (KO1 and KO2) had a 1 bp insertion that created an immediate premature stop codon at the insertion site. The third clone (KO3) had a 17 bp deletion resulting in a frame-shift mutation and an early stop codon. This predicted stop codon occurred before the predicted catalytic His site in wild type MBOAT1. For *EMP2*, an unmodified wild type control ("Control") was isolated as well as one clone (EMP2^{KO}) that contained a homozygous 1-bp deletion resulting in a premature stop codon seven amino acids downstream.

Cell cycle profiling.—All cells were seeded to obtain 70-80% confluency in 6-well plates at time of harvest. Cells treated with DMSO were seeded at 30,000 cells per well. Cells treated with nutlin-3, palbociclib, pimasertib, or abemaciclib were seeded at 70,000 cells per well. HT-1080^{N} rtTA-CDKN1A cells treated with Dox or Dox + palbociclib were seeded at 70,000 cells per well, whereas HT-1080^{N} rtTA-MBOAT1^{WT} and rtTA-MBOAT1^{H381A} cells treated with Dox were seeded at 30,000 cells per well. HT-1080^{N} rtTA-MBOAT1^{WT} and rtTA-MBOAT1^{H381A} cells treated with Dox + palbociclib were seeded at 70,000 cells per well. HAP1^{N} MBOAT1 WT and KO cells were seeded at 50,000 cells per well in DMSO conditions and 100,000 cells per well for palbociclib treatment. The next day, cells were treated with the indicated conditions for 48 h prior to analysis. For all cell lines, the concentrations of treatment compounds were as follows: palbociclib (2 μM), nutlin-3 (10 μM), abemaciclib (1 μM), pimasertib (0.5 μM), Dox (0.1 μg/mL). Cells were then trypsinized using 0.25% trypsin-EDTA (Cat# 25200114, Thermo Fisher Scientific) and

washed 2x with 1.5 mL cold HBSS (Cat# 14025-134, Life Technologies). Cells were fixed in 70% ethanol and stored at −20°C for up to two weeks. Immediately prior to analysis, cells were brought to room temperature, washed 2x with 1.5 mL cold HBSS, and stained with solution containing RNase A solution (1:100 v/v, Cat# 19101, Qiagen, Hilden, Germany) and propidium iodide (PI) solution (1:20 v/v, Cat# P3566, Thermo Fisher Scientific) for 30 min at 37°C. After staining, cells were washed 1x with 1 mL of HBSS, resuspended in 500 μL HBSS, and strained through a filter cap FACS tube (Cat# 352235, Corning). Cell cycle status was quantified on an Attune NxT Flow Cytometer. Data was acquired using standard laser excitation (488 nm) and emission (filter 590/40 nm) settings. Cells were assigned to G1, S, and G2 phase based on PI fluorescence histograms analyzed with the FlowJo v10.8.1 cell cycle analysis tool and Dean-Jett-Fox model as described (https://docs.flowjo.com/flowjo/experiment-based-platforms/cell-cycle-univariate/).

Western blotting.—All cells were seeded in 6-well plates to obtain 70-80% confluence at time of harvest. Cells treated with DMSO were seeded at 30,000 cells per well. Cells treated with nutlin-3, palbociclib, pimasertib, or abemaciclib were seeded at 70,000 cells per well. HT-1080^{N} rtTA-CDKN1A cells treated with Dox or Dox + palbociclib were seeded at 70,000 cells per well, whereas HT-1080^{N} rtTA-$MBOAT1^{WT}$ and rtTA-$MBOAT1^{H381A}$ cells treated with Dox were seeded at cells per well. HT-1080^{N} rtTA-$MBOAT1^{WT}$ and rtTA-$MBOAT1^{H381A}$ cells treated with Dox + palbociclib were seeded at 70,000 cells per well. The next day, cells were treated with various drugs/conditions. For all cell lines, the concentrations of treatment compounds were as follows: palbociclib (2 μM), nutlin-3 (10 μM), abemaciclib (1 μM), pimasertib (0.5 μM), Dox (0.1 μg/mL). After 48 h, cells were washed 2x with 1.5 mL of cold HBSS and then scraped with a cell scraper (Cat# 07-200-364, Fisher Scientific). Cells were then pelleted and lysed in RIPA lysis buffer + 0.1% SDS with 1:200 protease inhibitor cocktail P8340 (Cat# P8340, Sigma-Aldrich). Harvested materials were incubated on ice for at least 30 min to ensure full lysis and then sonicated 10x at 20% amplitude using a Fisher Scientific Model 120 sonic dismembrator (Thermo Fisher Scientific). The lysates were centrifuged for 15 min at 18,213 x *g* at 4°C and supernatants were transferred to a new Eppendorf tube. Then, protein levels were quantified using the bicinchoninic acid (BCA) reagent (Cat# 23228, Thermo Fisher Scientific) per the manufacturer protocol in 96-well plate format. For the BCA assay, absorbance at 562 nm was measured using a Synergy Neo2 multimode plate reader (BioTek Instruments, Winooski, VT). Samples to be analyzed were prepared using 4x Laemmli Sample Buffer (Cat# 1610747, Bio-Rad, Hercules, CA) and run on 4-15% Mini-PROTEAN TGX precast protein gels (Cat# 4560184, Bio-Rad) in Tris-glycine running buffer (Cat# 1610772, Bio-Rad) at 100V. Proteins were transferred to nitrocellulose membranes using the iBlot2 system (Life Technologies). Blots were blocked for 1 h at room temperature in Intercept blocking buffer (Cat# 927-60001, LI-COR Biosciences, Lincoln, NE) incubated in primary antibody solution overnight at 4°C. Antibodies used were anti-ACSL4 (1:300, Cat# 22401-1-AP, Proteintech, Rosemont, IL), anti-Actin (1:4,000, C4, Cat# sc-47778, Santa Cruz Biotechnology, Dallas, TX), anti-Tubulin (1:5,000, DM1A, Cat# MS581P1, Thermo Fisher Scientific), anti-p21 (1:500, 12D1, Cat# #2947, Cell Signaling Technology, Danvers, MA), anti-Rb (1:1,000, G3-245, Cat# 554136, BD Biosciences, San Jose, CA), anti-phospho-Rb Ser807/811 (1:500, D2OB12, Cat #8516, Cell Signaling

Technologies), anti-p53 (1:1,000, DO-1, Cat# sc-126, Santa Cruz Biotechnology), anti-GPX4 (1:500, Cat# ab41787, Abcam) anti-GPX4 (1:1,000, EPNCIR144, Cat# 125066, Abcam), anti-eIF4E (1:1000, P-2, Cat# sc-9976, Santa Cruz Biotechnology), anti-xCT (1:500, D2M7A, Cat# 12691, Cell Signaling Technology), anti-FLAG (1:1,000, Cat# ab1257, Abcam), anti-HA tag (1:1000, C29F4, Cat# 3724, Cell Signaling Technology), and anti-FSP1 (1:1000, Cat# 20886-1-AP, Proteintech). All antibodies were diluted into 5 mL of Intercept blocking buffer. The next day, membranes were washed 3x for 10 min with Tris-buffered saline (TBS, Cat# 0788, ISC BioExpress, Kaysville, UT) containing 0.1% Tween 20 (TBST) at room temperature. Membranes were incubated in secondary antibody solution at room temperature for 45 min at a 1:15,000 dilution in 1:1 Intercept blocking buffer:TBST. Antibodies used were 680LT Donkey-anti-mouse (Cat# 926-68022, LI-COR), 680LT Donkey-anti-rabbit (Cat# 926-68023, LI-COR), 800CW Donkey-anti-mouse (Cat# 926-32212, LI-COR), or 800CW Donkey-anti-rabbit (Cat# 926-32213, LI-COR). After secondary antibody incubation, blots were washed 3x for 10 min with TBST and then imaged on a LI-COR Odyssey CLx imager at 169 μm resolution, high quality setting, and 0.0 mm focus offset.

RT-qPCR.—Cells were seeded in a 6-well plate at densities such that at the time of cell harvest, plates were 70-80% confluent. Cells treated with DMSO were seeded at 30,000 cells per well. Cells treated with nutlin-3, palbociclib, pimasertib, or abemaciclib were seeded at 70,000 cells per well. HT-1080^{N} rtTA-CDKN1A cells treated with dox or dox + palbociclib were seeded at 70,000 cells per well, whereas HT-1080^{N} rtTA-MBOAT1^{WT} and rtTA-MBOAT1^{H381A} cells treated with dox were seeded at 30,000 cells per well. HT-1080^{N} rtTA-MBOAT1^{WT} and rtTA-MBOAT1^{H381A} cells treated with dox + palbociclib were seeded at 70,000 cells per well. The next day, cells were treated with the indicated conditions for 48 h prior to analysis. For all cell lines, the concentrations of treatment compounds were as follows: palbociclib (2 μM), nutlin-3 (10 μM), abemaciclib (1 μM), pimasertib (0.5 μM), dox (0.1 μg/mL). Next, cells were washed twice in warm PBS (0.5 mL) and then scraped into 0.5 mL PBS. Cells were lysed using a Qiashredder column (Cat# 79654, Qiagen). RNA was isolated using the RNeasy Plus RNA Extraction Kit (Cat# 74134, Qiagen) per manufacturer protocol and stored at −80°C. cDNA was generated with the TaqMan Reverse Transcriptase Kit (Cat# N8080234, Life Technologies) using 100 ng of RNA template. Quantitative PCR reactions were prepared with SYBR Green Master Mix (Cat# 4367659, Life Technologies) and run on an Applied Biosystems QuantStudio 3 real-time PCR machine (Thermo Fisher Scientific). Relative transcript levels were determined using the ΔΔCT method by normalizing the expression of the gene of interest to the expression levels of either *ACTB* or *GADPH*. qPCR primer sequences are provided in Table S1.

Glutathione measurements.—Total glutathione was assayed as described.[4] 30,000 (DMSO) or 70,000 (nutlin-3 or palbociclib) HT-1080^{N} cells were seeded in 6-well plates. The next day, cells were treated with DMSO, nutlin-3 (10 μM), or palbociclib (2 μM) and then returned to the incubator for 48 h. 40 h later, a separate group of cells were treated with erastin2 (2 μM) for 8 h such that each condition ended its treatment time simultaneously. Following this treatment, cells were washed once with HBSS and scraped into MES buffer

containing 1 mM EDTA. Samples were sonicated ten times with one second pulses at maximum amplitude on a Fisher Scientific Model 120 Sonic Dismembrator (Thermo Fisher Scientific) at 50% total amplitude. Lysates were centrifuged at >15,000 x *g* for 15 min at 4°C. Then samples were incubated for 5 min at room temperature in an equal volume of 12.5 M metaphosphoric acid (Cat# AC21922-1000, Thermo Fisher Scientific). Lysates were then centrifuged at >20,000 x *g* for 3 min at room temperature and the resultant supernatants were collected and stored at −20°C. Total glutathione was measured using the Cayman Glutathione Assay kit (Cat# 703002, Cayman Chemical) per the manufacturer's instructions. After 30 min incubation, absorbance was measured using a Synergy Neo2 plate reader (BioTek) at 402 nm.

C11 BODIPY 581/591 analysis.—Confocal imaging was performed as described.[8] Briefly, HT-1080 cells were seeded in 6-well tissue culture plates containing glass coverslips. 4 x 10^4 cells were seeded for the DMSO condition and 8 x 10^4 cells were seeded for the palbociclib condition. The next day, cells were treated with DMSO or palbociclib (2 μM) and returned to the incubator for 48 h. Then, DMSO or RSL3 (5 μM) was added for 1 h. Cells were then washed with pre-warmed HBSS. C11 BODIPY 581/591 (C11, 5 μM final concentration) and DAPI at 0.1 μg/mL final concentration were diluted in HBSS. 300 μL of the C11/DAPI/HBSS solution was added to cells for 10 min at 37°C. This solution was then aspirated and 1 mL of fresh HBSS was added to cells. Coverslips were mounted onto glass microscopy slides, which were imaged on a Zeiss Observer Z1 confocal microscope with a confocal spinning-disk head (Yokogawa, Tokyo, Japan), PlanApoChromat 63×/1.4 NA oil immersion objective, and a Cascade II:512 electron-multiplying (EM) CCD camera (Photometrics, Tucson, AZ). Three biological replicates were imaged per condition, with ten different regions of interest (ROI) captured per slide. Representative images are shown. Images were processed in ImageJ. Brightness for all images was auto adjusted based on images with the brightest signal.

For HT-1080^N rtTA-CDKN1A cells, C11 oxidation was detected using a BioTek Lionheart microscope. Here, cells were seeded in 96-well plates at 1,500 cells/well (for DMSO treatment) or 3,000 cells/well (for Dox, palbociclib, or Dox + palbociclib treatment). Two wells were seeded per condition. The next day, media were removed, and 200 μL of fresh growth media containing DMSO, Dox (0.1 μg/mL), palbociclib (2 μM), or Dox + palbociclib were added to the wells. 48 h later, media were removed and fresh media containing either DMSO or RSL3 (5 μM) were added to the cells such that each pretreatment condition (DMSO, Dox, palbociclib, Dox + palbociclib) had one well with DMSO and one well with RSL3. One hour later, media were removed from the wells, and each well was washed with 100 μL of warm sterile PBS. C11 (5 μM final concentration) and Hoechst (1 μg/mL final concentration) (Cat# H1399, Fisher Scientific) were diluted in warm PBS. 50 μL of the solution was added to each well for 10 min at 37°C. Then, the solution was removed and 100 μL PBS added to each well. The plate was immediately imaged on a BioTek Lionheart imager. The automated imager acquired one image per well using a 20x objective with a correction collar of 1.25 mm. DAPI (excitation: 377 nm, emission: 447), Texas Red (excitation: 586 nm, emission: 647), and GFP (excitation: 469 nm, emission: 525) filter cubes were used. Images were quantified using Gen5 v3.10 software (BioTek) to

determine oxidized/non-oxidized (ox/non-ox) C11 ratio per cell. Ox/non-ox ratio is reported per each cell analyzed, summed across three replicates. More than 100 cells were quantified per condition.

For 786-O and MDA-MB-231 cells C11 oxidation was examined as follows. Cells were seeded in 10 cm plates at the density of 800,000 cells/plate and treated with vehicle control or palbociclib (1 μM) for 48 h. After pretreatment, cells were trypsinized, seeded into 12-well plates (80,000 cells per well), and treated with ferroptosis-inducing compounds ± inhibitors. At the end of treatment, the culture medium was collected. Cells were then washed with 300 μL PBS and the PBS was combined with culture medium. Cells were then trypsinized using 100 μL trypsin and neutralized with the collected culture medium. After centrifugation at 500 x *g* for 5 min, cells were resuspended in 300 μL PBS containing C11 (1 μM) for 30 min at 37°C. Then cells were resuspended in 180 μL PBS and detected by flow cytometry using BD fortessa X-20 cytometer. Live single cells were gated and the geometric means of FITC (green) and PE (red) intensity were acquired using FlowJo software. The green-to-red ratio was then calculated to indicate lipid peroxidation.

RNA-sequencing.—HT-1080^{N} cells were seeded in 6-well plates at 30,000 cells (DMSO) or 70,000 cells (palbociclib or pimasertib treatment). The next day, growth media was removed and replaced with 2 mL media containing DMSO, palbociclib (2 μM), or pimasertib (0.5 μM). After 48 h, RNA was extracted as described above. RNA quality was measured at the Stanford Protein and Nucleic Acid Facility using the Eukaryote Total RNA nanochip (Agilent Technologies). Library generation, read sequencing, and data cleanup were performed by Novogene.[64] Briefly, an Illumina HiSeq 4000 platform was used to sequence bases, and reads were excluded if indeterminate bases consisted of >10% of the read or >50% of the bases had a quality score of less than five. The raw image files from the high-throughput sequencing were transformed into sequenced reads using CASAVA base recognition. Reads were then mapped to the reference genome (hg19) using the STAR aligner. Expression of each mRNA was calculated and reported as fragments per kilobase of transcript sequence per million base pairs sequenced (FPKM). The change in FPKM was compared between groups (e.g., DMSO versus palbociclib) and differential expression was analyzed using the DESeq2 R package. FDR correction was performed using the Benjamini-Hochberg method. Differentially expressed genes that met an FDR cutoff threshold of $q < 0.05$ were reported.

TCGA analysis.—The TCGA-SARC dataset was accessed on 8/7/23. The following search terms were used: “Available variation data IS ssm AND Project Id IS TCGA-SARC AND Gene IS RB1”. 149 cases met these criteria, but RNA sequencing reads were only available for 147 tumors. 25 tumors were classified as Rb mutant with VEP impact level “high”, indicating that the mutation was predicted to have severe consequence (e.g., frame-shift mutation, stop codon gained, etc.). Sequencing data for 123 WT tumors was available. The FPKM scores of the indicated genes is displayed. Displayed p-values denote the result of 2-tailed Student’s t-tests.

siRNA transfection: siRNAs were purchased from Integrated DNA Technologies (IDT, Newark, NJ). The siRNA used were hs.Ri.MBOAT1.13.3, hs.Ri.EMP2.13.2 and

hs.Ri.EMP2.13.3. AllStars Negative Control siRNA (siNTC, Cat# 1027280, Qiagen) was used as a validated non-targeting siRNA control for all experiments. HT-1080^{N} and Caki-1^{N} cells were seeded at 25,000 cells per well (in 12-well plates) or 75,000 cells per well (in 6-well plates). T98G^{N} and A375^{N} cells were seeded at 75,000 cells per well in 6-well plates, treated with hs.Ri.MBOAT1.13.3 for 48 h, and then trypsinized and seeded into 96-well plates at a density of 6,000 cells per well. The following day, the indicated doses of RSL3 were added to each well. For si-NTC, si-*MBOAT1*, and si-*EMP2*, 10 pmol of siRNA per 250 μL of transfection reagent was used. siRNA was combined with 2.5 μL of Lipofectamine RNAiMAX transfection reagent (Cat# 13778075, Life Technologies) and 250 μL of OptiMEM reduced serum growth medium (Cat# 31985070, Thermo Fisher Scientific) in a new 12-well plate. For 6-well plates, the same ratios were used with double the amount of each reagent. The transfection mixture was incubated in the well for at least 15 min, and then cell suspensions were carefully added to each well. For relevant experiments/conditions, palbociclib was added at time of seeding at 2 μM. 48 h later, growth medium was removed and replaced with medium containing SYTOX Green (20 nM) and the indicated concentration of RSL3 and/or ferrostatin-1. For RNA measurements, cells were scraped 48 h after transfection and analyzed. (See “RT-qPCR” for relevant details.)

Untargeted lipidomic analysis.—HT-1080^{N} rtTA-MBOAT1^{WT} and HT-1080^{N} rtTA-MBOAT1^{H381A} cells were seeded in 10 cm plates. For both cell lines, 300,000 cells/plate were used for the DMSO and Dox treatment conditions, and 600,000 cells/plate were used for palbociclib or Dox + palbociclib treatment conditions. HT-1080^{N} ACSL4 WT, KO1, and KO2 cells were seeded in 10 cm plates. For all cell lines, 300,000 cells/plate were used for the DMSO condition, and 600,000 cells/plate were used for the palbociclib condition. One day after seeding, cell culture media were changed to fresh media containing DMSO, Dox (0.1 μg/mL), palbociclib (2 μM), or Dox + palbociclib. 48 h later, cells were washed 2x with 5 mL of warm PBS and then scraped into PBS using Corning cell lifters (Cat# 07-200-364, Fisher Scientific). 100 μL of cell extract was removed for protein quantification using the BCA assay (Cat# 23252, Thermo Fisher Scientific). Lipids were extracted from the cells using a modified Folch extraction, Final: 2:1:1 CHCl3:MeOH:PBS. Chloroform (Cat# 366927) and methanol (Cat# 34860-4L-R) were obtained from Sigma-Aldrich. All reagents used were HPLC grade. Lipid extracts were shaken vigorously for 10 s, and then centrifuged at 350 x *g* for 5 min at 4°C. The organic (lower) phase was removed into a fresh glass vial and then dried under N2. Lipids were stored at −80°C until run on the mass spectrometer.

On the morning of the analysis by mass spectrometry, lipids were resuspended in 100 μL of 9:1 MeOH:toluene. HPLC grade toluene was obtained from Sigma-Aldrich (Cat# 34866). The samples were then run as previously described.[65] Briefly, buffer A was 60:40 acetonitrile (ACN):H2O, while buffer B was 90:10 isopropanol (IPA):ACN. In positive mode the additives were 0.1% formic acid in buffer A and 10 mM ammonium formate and 0.1% formic acid in buffer B. In negative mode, the additive was 10 mM ammonium acetate. Each run was for 15 min with the following conditions: 0 min 85% (A); 0-2 min 70% (A); 2-2.5 min 52% (A); 2.5-11 min 18% (A); 11-11.5 min 1% (A); 11.5-12 min 1% (A); 12-12.1 min 85% (A). For MBOAT1 overexpression experiments, an Acquity UPLC

CSH C18 column (100 x 2.1 mm; 1.7 μm, Cat# 186005297) maintained at 65°C was used in for high-performance liquid chromatography (HPLC) analysis. For HT-1080^{N} Control and *ACSL4* gene-disrupted cells, an Agilent ZORBAX RR Eclipse Plus C18 column (95Å, 4.6 x 100 mm, 3.5 μm, part number 959961-902) maintained at 65°C was used in the HPLC phase. For HPLC runs on this column, an additional five minutes of equilibration was added (15-20 min) at 85% (A). Samples were maintained at 4°C in the autosampler for the duration of the experiment.

An Agilent (Santa Clara, CA) 6545 quadrupole time of flight (qTOF) mass spectrometer was used to acquire data in negative electrospray ionization mode with the parameters: mass range *m/z* 100-1700, spray voltage 4k V, drying gas flow rate 6 L/min, gas temperature 250°C, in full scan MS1 mode. The instrument was tuned and calibrated prior to each run._Agilent .d raw files were converted to mzML using ProteoWizard MSConvert software. Peaks were then aligned, grouped, and integrated using the xcms R package (BioConducter version 3.16). Isotope and adduct assignments were made using the R package CAMERA (BioConducter version 3.16). For lipidomics experiments in ACSL4 Control and KO cells, 3832 peaks were detected after xcms analysis. The AUC/mg protein levels of 1546 peaks were significantly changed ± palbociclib treatment in Control cells, as determined by two-tailed Student's t-test ($P < 0.05$). 443 remained significant after Benjamini-Hochberg FDR testing with a strict cutoff of $q < 0.01$. Of those, 313 peaks were not altered by palbociclib treatment in ACSL4$^{KO1/2}$ cell lines (two-tailed Student's t-test, $p < 0.05$). Values are reported in the Supplemental Data File S2.

Targeted MS/MS verification.—Select lipids from the *MBOAT1* overexpression dataset and the ACSL4^{KO} dataset were validated by targeted MS/MS run on an Agilent 6545 qTOF. MS analysis was performed in positive mode and negative mode. Chromatography and instrument parameters were identical to those used for the untargeted lipidomics (see above) with the following additional settings for MS2. For all lipids, a collision energy of 20 eV was used and the isolation window was set to narrow (~1.3 *m/z*). For identification of PE P-16:0/20:4 and PE P-16:0/22:6, 30,000 HT-1080^{N} cells were seeded in 6-well plates for DMSO treatment, and or 70,000 cells were seeded for palbociclib (2 μM) treatment. The next day, growth media were replaced with 2 mL of media containing either DMSO or palbociclib. 48 h later, lipids were extracted as described above for untargeted lipidomic analysis. 10 μL of lipid extract was run on the qTOF. In negative mode, analytes with *m/z* of 722.5127 and 746.5127 were fragmented. In positive mode, *m/z* 724.5273 and *m/z* 748.5273 were fragmented and analyzed. Only one species with *m/z* 722.5127 that was fragmented also displayed an increased abundance in HT-1080^{N} cells treated with palbociclib compared to those treated with DMSO. The same was true of *m/z* 746.5127. The MS/MS spectra of these two ions was analyzed in detail. In negative mode, the *sn*-2 chains of plasmalogen PE lipids can be identified as described.[66,67] Based on the product ions detected, as well as their relative abundances, these two species could be conclusively identified as PE P-16:0/20:4 and PE P-16:0/22:6, as previously described (https://www.biorxiv.org/content/10.1101/2021.01.20.427444v1.full.pdf).

For identification of *m/z* 700.5287, 30,000 HT-1080^{N} rtTA-MBOAT1^{WT} and HT-1080^{N} rtTA-MBOAT1^{H381A} mutant cells were seeded into one well of a 6-well plate. The next day,

cells were treated with either Dox (0.1 μg/mL) or an equivalent volume of sterile H_2O. 48 h later, lipids were extracted as described above. 10 μL of lipid solution was run on the qTOF as described above. In negative mode, species with *m/z* 700.5287 were fragmented and analyzed. In positive mode, species with *m/z* of 702.543 were fragmented and analyzed. Species were selected for further analysis if their abundance increased in HT-1080^N rtTA-$MBOAT1^{WT}$ cells treated with Dox, but not in HT-1080^N rtTA-$MBOAT1^{H381A}$ cells treated with Dox. In negative mode, one species met these criteria. In positive mode no interpretable spectra for species with *m/z* 702.543 could be obtained. Therefore, the identity of this species could not be exclusively assigned. However, the results from the negative mode fragmentation indicated that this species was a PE phospholipid with 1-*O*-alkyl 16:1 on its *sn*-1 chain and 18:1 on its *sn*-2 chain. It was therefore annotated PE *a*-16:1/18:1 where a denotes the alkyl bond. For all MS/MS experiments, Agilent .d files were analyzed using Agilent MassHunter Qualitative Analysis software.

Untargeted lipidomics in Ctrl and $EMP2^{KO}$ cells.—On day 0, 300,000 HT-1080^N Control or $EMP2^{KO}$ cells were seeded in 10 cm^2 plates for DMSO treatment. For palbociclib treatment, 600,000 cells were seeded. On day 1, palbociclib (2 μM), or an equal volume of DMSO (negative control), was added to the growth medium. 48 h later (day 3), cells were washed with 3 mL of 4°C 1X PBS and scraped into 0.5 mL of cold PBS. Cells were pelleted at 450 x *g* for 5 min, supernatant was aspirated, and pellets were stored at −80°C. Before extraction, cell pellets were thawed on ice for 30 min and resuspended in 50 μL PBS. 3 μL of SPLASH® LIPIDOMIX® internal standard (Cat# 330707-1EA, Avanti Polar Lipids) dissolved in methanol was added directly to each suspension. Lipids were extracted by adding 1.25 mL of tert-butyl methl ether (Cat# 34875-1L, Sigma Aldrich) and 0.375 mL of methanol (Cat# A452-4, Fisher Scientific). The mixture was incubated on an orbital mixer for 1 h (RT, 32 rpm). To induce phase separation, 0.315 mL of H_2O was added, and the mixture was incubated on an orbital mixer for 10 min (room temperature, 32 rpm). Samples were centrifuged (RT, 2 min, 15,000 x *g*). Upper organic phase was collected and subsequently dried *in vacuo* (Eppendorf concentrator 5301, 1 ppm).

Dried lipid extracts were reconstituted in chloroform/methanol (150 μL, 2:1, v/v) and 20 μL of each extract was transferred to HPLC vials containing glass inserts. Quality control samples were generated by mixing equal volumes of each lipid extract followed by aliquotation in 20 μL aliquots. Aliquoted extracts were dried *in vacuo* (Eppendorf concentrator 5301, 1 ppm) and redissolved in 20 μL of 2-propanol (Cat# 1.02781.4000, Supelco, St. Louis, MO) for injection.

Lipids were separated by reversed phase liquid chromatography on a Vanquish Core (Thermo Fisher Scientific, Bremen, Germany) equipped with an Accucore C30 column (150 x 2.1 mm; 2.6 μm, 150 Å, Thermo Fisher Scientific, Bremen, Germany). Lipids were separated by gradient elution with solvent A (MeCN (Cat# A955-4, Fisher Chemical)/H_2O (Cat# W6-4, Fisher Chemical), 1:1, v/v) and B (2-propanol/MeCN/H_2O, 85:10:5, v/v) both containing 5 mM NH_4HCO_2 (Cat# 70221-25G-F, Sigma-Aldrich) and 0.1% (v/v) formic acid (Cat# A117-50, Fischer Chemical). Separation was performed at 50°C with a flow rate of 0.3 mL/min using the following gradient: 0-15 min – 25 to 86 % B (curve 5), 15-21 min

– 86 to 100 % B (curve 5), 21-32 min – 100 % B isocratic, 32-32.1 min – 100 to 25 % B (curve 5), followed by 5.9 min re-equilibration at 25 % B.

Reversed phase liquid chromatography was coupled on-line to a Q Exactive Plus Hybrid Quadrupole Orbitrap mass spectrometer (Thermo Fisher Scientific, Bremen, Germany) equipped with a HESI probe. Mass spectra were acquired in positive and negative modes with the following ESI parameters: sheath gas, 40 L/min; auxiliary gas, 10 L/min; sweep gas, 1 L/min; spray voltage, 3.5 kV (positive ion mode) and −2.5 kV (negative ion mode); capillary temperature, 250 °C; S-lens RF level, 35; aux gas heater temperature, 370 °C.

Data acquisition for lipid identification was performed in quality control samples by acquiring data in data dependent acquisition mode (DDA). DDA parameters featured a survey scan resolution of 140,000 (at *m/z* 200), AGC target 1e6 Maximum injection time 100 ms in a scan range of *m/z* 240-1200. Data dependent MS/MS scans were acquired with a resolution of 17,500, AGC target 1e5, Maximum injection time 60 ms, loop count 15, isolation window 1.2 *m/z* and stepped normalized collision energies of 10, 20 and 30 %. A data dependent MS2 was triggered when an AGC target of 2e2 was reached followed by a Dynamic Exclusion for 10 s. All isotopes and charge states > 1 were excluded. All data was acquired in profile mode.

For deep lipidome profiling, iterative exclusion was performed using the IE omics R package.[68] This package generates a list for already fragmented precursors from a prior DDA run that can be excluded from subsequent DDA runs ensuring a higher number of unique MS/MS spectra for deep lipidome profiling. After the initial DDA analysis of a quality control sample, another quality control sample was measured but excluding all previously fragmentated precursor ions. Parameters for generating exclusion lists from previous runs were – RT window = 0.3; noiseCount = 15; MZWindow = 0.02 and MaxRT = 36 min. This workflow was performed one time to achieve a total of two DDA analyses of a quality control sample in positive and two DDA analysis in negative ionization mode. Data for lipid quantification was acquired in *Full MS* mode with following parameters – scan resolution of 140,000 (at *m/z* 200), AGC target 1e6 Maximum injection time 100 ms in a scan range of *m/z* 240-1200.

Lipostar (version 1.0.6, Molecular Discovery, Hertfordshire, UK) equipped with in house generated structure database featuring fatty acids with no information on double bond regio- or stereoisomerism covering glycerolipid, glycerophospholipid, sphingolipid and sterol ester lipid classes. The raw files were imported directly with a Sample MS Signal Filter Signal Threshold = 1000 for MS and a Sample MS/MS Signal Filter Signal Threshold = 10. Automatic peak picking was performed with an m/z tolerance = 5 ppm, chromatography filtering threshold = 0.97, MS filtering threshold = 0.97, Signal filtering threshold = 0. Peaks smoothing was performed using the Savitzky-Golay smoothing algorithm with a window size = 3, degree = 2 and multi-pass iterations = 3. Isotopes were clustered using a m/z tolerance = 5 ppm, RT tolerance = 0.25 min, abundance Dev = 40%, max charge = 1. Peak alignment between samples using an m/z tolerance = 5 ppm and an RT tolerance = 0.25 min. A gap filler with an RT tolerance = 0.05 min and a signal filtering threshold = 0 with an anti-Spike filter was applied.

For lipid identification, a “MS/MS only” filter was applied to keep only features with MS/MS spectra for identification. Triacylgylcerols, diacylglycerols and sterol esters were identified as [M+NH4]+ adducts. Lysophosphatidylcholines, lysophosphatidylethanolamines, Acyl-, ether- and vinyl ether-PE, ceramides and Sphingomyelins were analyzed as [M+H]+ adducts. Phosphatidylserines, and phosphatidylinositols were analyzed as [M-H]− adducts. Acyl-, ether- and vinyl ether-Phosphatidylcholines were identified as [M+HCOO]− adducts. The following parameters were used for lipid identification: 5 ppm precursor ion mass tolerance and 20 ppm product ion mass tolerance. Automatic approval was performed to keep structures with quality of 3-4 stars. Identifications were refined using manual curation and Kendrick mass defect analysis and lipids that were not following these retention time rules were excluded as false positives. Quantification was performed by peak integration of the extracted ion chromatograms of single lipid adducts of these high confidence lipids. Peak integration was manually curated and adjusted. Identified lipids were normalized to peak areas of added internal standards to decrease analytical variation and eventually normalized to protein concentrations of cell pellets after lipid extraction.

Statistical analysis of EMP2^{KO} lipidomics.—678 total lipids were detected. Two-tailed t-tests followed by Benjamini-Hochberg FDR testing was performed comparing HT-1080^{N} Control to EMP2^{KO} cells, with an FDR cutoff of $q < 0.01$. When comparing DMSO to palbociclib treatment in Control cells, 2-tailed t-tests followed by Benjamini-Hochberg FDR testing was performed. Only 5 lipids were significant with an FDR cutoff of $q < 0.01$ and so an FDR cutoff of $q < 0.05$ was used instead. Lipids were included if palbociclib treatment and EMP2^{KO} altered the lipid in the same direction (positive vs negative). Lipids were included in the final count if they were not significantly different in the DMSO and palbociclib conditions in EMP2^{KO} cells (2-tailed t-test, $p > 0.05$). Lipid pathway enrichment was assessed using the Bioinformatics Methodology For Pathway Analysis (BioPAN) webtool (https://www.lipidmaps.org/biopan/). Networks were reported that contained >2 nodes. Principal component analysis was performed using MetaboAnalyst 5.0.[69] Data was uploaded in .csv format to the Statistical Analysis [one factor] tool. Data was transformed using the “Log transformation (base 10)” setting and then scaled using the “Auto Scaling (mean-centered and divided by the standard deviation of each variable)” setting. PCA scores and loadings data were exported in .csv format and graphed using GraphPad Prism.

Analysis of CTRP dataset.—Data from the Cancer Therapeutics Response Portal (CTRP) v2.1 dataset (https://ocg.cancer.gov/ctd2-data-project/broad-institute-screening-dependencies-cancer-cell-lines-using-small-molecules-0) was accessed on June 12th, 2023. The data for statistically significant correlations between basal gene expression and small-molecule sensitivity across all cancer cell lines were extracted from the v21.data.gex_global_analysis.txt table and plotted using GraphPad Prism.

In vivo administration of palbociclib.—NOD-*scid* IL2Rgamma^{null} (NSG) mice were obtained commercially (Jackson Laboratory, stock no. 005557, Bar Harbor, ME). HT-1080^{N} tumor cells were mixed with Matrigel (Cat# 356231, Corning) in a 1:1 ratio such that 2.5

x 10^6 cells in 200 μL of media was mixed with 200 μL of Matrigel. Tumors were injected into both the left and right flanks of mice and allowed to incubate until reaching an average volume of 100 mm^3 across all tumors. Mice were then divided into cohorts that received either vehicle control (methocellulose grade A4M 0.5% w/v in milliQ water), or palbociclib (Cat# P-7788, LC Laboratories, Woburn, MA) dissolved in vehicle at 25 mg/mL. In the first experiment, mice were dosed at 100 mg/kg daily for 5 d by oral gavage. Mice were sacrificed on day 6 according to IACUC regulations. Tumors were extracted and dissociated for analysis of mRNA and lipid expression, which were performed as above. We were unable to successfully extract assay-quality mRNA for two tumors, and so mRNA from nine tumors (vehicle) and seven tumors (palbociclib) were analyzed in downstream analyses.

Combination of palbociclib and compound 28.—NOD-*scid* IL2Rgamma^{null} (NSG) mice were obtained from the Jackson Laboratory (Stock No. 005557, Bar Harbor, ME). HT-1080^N tumor cells were mixed with Matrigel (Cat# 356231, Corning) in a 1:1 ratio such that 2.5 x 10^6 cells in 200 μL of media was mixed with 200 μL of Matrigel. Tumors were injected into both the left and right flanks of mice and allowed to incubate until reaching an average volume of 100 mm^3 across all tumors. Mice were then divided into cohorts that received either vehicle control (methocellulose grade A4M 0.5% w/v in milliQ water), or palbociclib (Cat# P-7788, LC Laboratories, Woburn, MA) dissolved in vehicle at 25 mg/mL. In a first experiment with palbociclib or vehicle alone, mice were dosed at 100 mg/kg daily for 5 d by oral gavage. Mice were sacrificed on day 6 according to IACUC regulations. Tumors were extracted and dissociated for analysis of mRNA and lipid expression.

For experiments testing the palbociclib and compound 28 combination, the vehicle for palbociclib was methocellulose as described above. For compound 28, a solution of methocellulose (0.5% w/v, Cat# ME137-100GM, Spectrum Chemicals, West Compton, CA) with Tween80 (0.5% w/v, Cat# P1754-500ML, Millipore Sigma, Burlington, MA) dissolved in ddH_2O was used as the vehicle. This solution was termed MCT. Polyethylene glycol 400 (PEG400, Cat# PO110-500MLGL, Spectrum Chemical) and ethanol (Cat. 493546-1L, Sigma Aldrich) were combined in a 1:3 ethanol:PEG400 ratio (ethanol/PEG400). The final vehicle for compound 28 contained 40:60 ethanol/PEG400:MCT, and compound 28 was dissolved at 15 mg/mL. Female 3-month-old NSG mice (Stock No. 005557, Jackson Laboratories) were injected with HT-1080 cells as above, and the experiment began when tumors reached an average volume of 100 mm^3 (day 0). Mice were dosed with compound 28 (60 mg/kg) and/or palbociclib (100 mg/kg) on the following schedule. Palbociclib or vehicle control was dosed on days 2, 3, 9 and 10. Compound 28 or appropriate vehicle control was dosed on days 5, 6, 12, and 13. Animals began to reach humane endpoints and so mice were sacrificed and tissues harvested on day 17. Analysis of lipid levels was performed as described above.

Compound 28 target engagement.—Tumors protein was extracted from approximately 25 mg of tumor sample in RIPA lysis buffer + 0.1 % SDS with 1:200 protease inhibitor cocktail P8340 (Cat# P8340, Sigma-Aldrich). Samples were centrifuged for 15 min at 18,213 x *g* at 4°C and supernatants were transferred to a new Eppendorf tube. Then, protein levels were quantified using the bicinchoninic acid (BCA) reagent

(Cat# 23228, Thermo Fisher Scientific) per the manufacturer protocol in 96-well plate format. For the BCA assay, absorbance at 562 nm was measured using a Synergy Neo2 multimode plate reader (BioTek Instruments, Winooski, VT). Samples were then prepared with 4X Bolt® LDS Sample Buffer (Cat# B0007, Life Technologies) and 10x Bolt Sample Reducing Agent (Cat# 0009, Thermo Fisher Scientific). 10 μg of protein was then run on a Bolt® 4-12% Bis-Tris Plus Gel, 15 wells (Cat# NW04125BOX, Life Technologies) for 2 h at 95 V. Proteins were transferred to nitrocellulose membranes using the iBlot2 system (Life Technologies). Blots were blocked for 1 h at room temperature in Intercept blocking buffer (Cat# 927-60001, LI-COR Biosciences, Lincoln, NE) incubated in primary antibody solution overnight at 4°C. anti-Tubulin Primary antibodies were anti-Tubulin (1:5,000, DM1A, Cat# MS581P1, Thermo Fisher Scientific) and anti-GPX4 (1:500, EPNCIR144, Cat# 125066, Abcam). Membranes were then incubated in secondary antibody and imaged as above in “Western blotting”.

Immunohistochemistry for 4-HNE.—Isolated tumor xenografts as well as normal liver were fixed in 10% neutral buffered formalin. Cassettes were then submerged in 70% ethanol for 24 h. Subsequent sample preparation and staining was performed at the Stanford Animal Histology core facility. Paraffin embedding was performed by submerging samples in 70% ethanol (40 min, 40°C), 95% ethanol (2X 40 min, 40°C), 100% ethanol (2x 40 min, 40°C), xylene (3x 40 min, 40°C), and subsequently submerged in paraffin (2x 40 min, 60°C). Samples were cut to a thickness of approximately 5 microns and affixed onto glass slides (UNSPSC Code 41110000, Springside Scientific LLC, Durham, NC). Once dry, the tissue slices were deparaffinized and antigen retrieval was performed by boiling samples in citric acid (pH 6.0) for 20 min. Samples were washed in TBS for 1 min and blocked in avidin blocking solution (Cat# 927301, BioLegend, San Diego, CA) for 10 min. Slides were washed with TBS for 1 min and then blocked in biotin blocking solution (Cat# 927301, BioLegend) for 10 min. Finally, slides were washed for 1 min with TBS and then blocked in 3% goat serum (gift from Stanford Veterinary Service Center) in TBS for 10 min.

For 4-HNE, slides were incubated overnight at 4°C with an anti-4-hydroxynonenol (4-HNE) primary antibody (Cat# ab46545, AbCam) at a concentration of 1:300 in 3% goat serum in TBS with 0.5% Tween. The next day, slides were washed in TBS for one minute, blocked with 3% Peroxide block (Cat# H312-500, Thermo Fisher Scientific) diluted 1:10 in PBS for 10 min, and then washed three times with TBS for three min. Ready to use (no dilution) BT goat anti-rabbit secondary antibody (Cat# ab64256, AbCam) was added to the slides for 45 min at room temperature. 3x TBS washes (3 min each) were performed, and then slides were incubated with streptavidin-HRP tertiary antibody (Cat# N100, Thermo Fisher Scientific) at 1:1,000 dilution for 45 min at RT. Slides were washed three times with TBS for 3 min each. DAB chromogen (Cat# ab64238, AbCam) was added to the slides for 5 min, and slides were washed in deionized water for 1 min. Ten (4-HNE) images were captured per slide. Representative images are shown.

Quantification of 4-HNE staining.—A python script was developed to quantify the intensity of brown (4-HNE positive) pixels in each image. Python version 3.10 was used. Code was developed and run in PyCharm (2021.1.1). Briefly, RGB images were converted

to YCoCg color space, as the Co vector was found to be a good representation of the staining data. The Co pixel data (default 0 to 255) was normalized from 0 to 1 (subsequently termed “intensity value”) by dividing all values by 255. Pixels were called as 4-HNE positive ($4HNE^+$) if they met a minimum intensity threshold determined empirically. Flood fill,[70] a background subtraction strategy, was used to remove background pixels from the analysis. The intensity values of 4HNE+ pixels were averaged to create a single intensity score per image. The intensity scores across all 380 images (10 regions of interest per tumor, 8 or 10 tumors per condition) were normalized and plotted. Statistical testing was performed comparing the groups using one-way ANOVA with Tukey’s post-hoc tests.

QUANTIFICATION AND STATISTICAL ANALYSIS

Lethal fraction calculations and statistical analyses were performed using Microsoft Excel 14.6.0 (Microsoft Corporation, Redmond, WA). Flow cytometry data were analyzed using FlowJo 10.6.1 (FlowJo LLC, Ashland, OR). C11 BODIPY 581/591 images acquired using the Lionheart imager were analyzed with Gen5 v3.10 software (BioTek). Some images were analyzed using ImageJ (https://imagej.net/ij/index.html). Graphing was performed using Prism 9 (GraphPad Software, La Jolla, CA). Figures were assembled using Adobe Illustrator (Adobe Systems, San Jose, CA). Details of experiment design and statistical testing (where appropriate) used can be found in the main text, figure legends, and Methods.

Supplementary Material

Refer to Web version on PubMed Central for supplementary material.

ACKNOWLEDGEMENTS

We thank P. Beltran and C. Stahlhut for providing compound 28 and advice, S. Terrel, T. Hammond, L. Pope, E. Peterson and N. Terrell for assistance, J. Carette for reagents, J. Skotheim for advice, and L. Magtanong and members of the Dixon lab for comments on the manuscript. Certain constructs were obtained from Addgene. J.A.O. is a Chan Zuckerberg Biohub – San Francisco Investigator. This work was supported by awards from the National Institutes of Health to J.R. (1F31CA265146), Z.T.S., (R01CA262439), J.A.O. (R01GM112948), J.S. (R01CA228413), and S.J.D. (2R01GM122923), an award from the American Cancer Society (RSG-21-017-01-CCG) to S.J.D., and funding from Ferro Inc. to S.J.D.

REFERENCES

1. Stockwell BR (2022). Ferroptosis turns 10: Emerging mechanisms, physiological functions, and therapeutic applications. Cell 185, 2401–2421. 10.1016/j.cell.2022.06.003. [PubMed: 35803244]
2. Jiang X, Stockwell BR, and Conrad M (2021). Ferroptosis: mechanisms, biology and role in disease. Nat Rev Mol Cell Biol. 10.1038/s41580-020-00324-8.
3. Zhang Y, Tan H, Daniels JD, Zandkarimi F, Liu H, Brown LM, Uchida K, O'Connor OA, and Stockwell BR (2019). Imidazole Ketone Erastin Induces Ferroptosis and Slows Tumor Growth in a Mouse Lymphoma Model. Cell Chem Biol 26, 623–633 e629. 10.1016/j.chembiol.2019.01.008. [PubMed: 30799221]
4. Dixon SJ, Patel DN, Welsch M, Skouta R, Lee ED, Hayano M, Thomas AG, Gleason CE, Tatonetti NP, Slusher BS, and Stockwell BR (2014). Pharmacological inhibition of cystine-glutamate exchange induces endoplasmic reticulum stress and ferroptosis. Elife 3, e02523. 10.7554/eLife.02523. [PubMed: 24844246]
5. Yang WS, SriRamaratnam R, Welsch ME, Shimada K, Skouta R, Viswanathan VS, Cheah JH, Clemons PA, Shamji AF, Clish CB, et al. (2014). Regulation of ferroptotic cancer cell death by GPX4. Cell 156, 317–331. 10.1016/j.cell.2013.12.010. [PubMed: 24439385]

6. Doll S, Proneth B, Tyurina YY, Panzilius E, Kobayashi S, Ingold I, Irmler M, Beckers J, Aichler M, Walch A, et al. (2017). ACSL4 dictates ferroptosis sensitivity by shaping cellular lipid composition. Nat Chem Biol 13, 91–98. 10.1038/nchembio.2239. [PubMed: 27842070]
7. Kagan VE, Mao G, Qu F, Angeli JP, Doll S, Croix CS, Dar HH, Liu B, Tyurin VA, Ritov VB, et al. (2017). Oxidized arachidonic and adrenic PEs navigate cells to ferroptosis. Nat Chem Biol 13, 81–90. 10.1038/nchembio.2238. [PubMed: 27842066]
8. Magtanong L, Ko PJ, To M, Cao JY, Forcina GC, Tarangelo A, Ward CC, Cho K, Patti GJ, Nomura DK, et al. (2019). Exogenous Monounsaturated Fatty Acids Promote a Ferroptosis-Resistant Cell State. Cell Chem Biol 26, 420–432 e429. 10.1016/j.chembiol.2018.11.016. [PubMed: 30686757]
9. Perez MA, Magtanong L, Dixon SJ, and Watts JL (2020). Dietary Lipids Induce Ferroptosis in Caenorhabditiselegans and Human Cancer Cells. Dev Cell 54, 447–454 e444. 10.1016/j.devcel.2020.06.019. [PubMed: 32652074]
10. Wiernicki B, Dubois H, Tyurina YY, Hassannia B, Bayir H, Kagan VE, Vandenabeele P, Wullaert A, and Vanden Berghe T (2020). Excessive phospholipid peroxidation distinguishes ferroptosis from other cell death modes including pyroptosis. Cell Death Dis 11, 922. 10.1038/s41419-020-03118-0. [PubMed: 33110056]
11. Dixon SJ, and Pratt DA (2023). Ferroptosis: A flexible constellation of related biochemical mechanisms. Mol Cell 83, 1030–1042. 10.1016/j.molcel.2023.03.005. [PubMed: 36977413]
12. Magtanong L, Mueller GD, Williams KJ, Billmann M, Chan K, Armenta DA, Pope LE, Moffat J, Boone C, Myers CL, et al. (2022). Context-dependent regulation of ferroptosis sensitivity. Cell Chem Biol 29, 1409–1418 e1406. 10.1016/j.chembiol.2022.06.004. [PubMed: 35809566]
13. Chu B, Kon N, Chen D, Li T, Liu T, Jiang L, Song S, Tavana O, and Gu W (2019). ALOX12 is required for p53-mediated tumour suppression through a distinct ferroptosis pathway. Nat Cell Biol 21, 579–591. 10.1038/s41556-019-0305-6. [PubMed: 30962574]
14. Valente LJ, Tarangelo A, Li AM, Naciri M, Raj N, Boutelle AM, Li Y, Mello SS, Bieging-Rolett K, DeBerardinis RJ, et al. (2020). p53 deficiency triggers dysregulation of diverse cellular processes in physiological oxygen. J Cell Biol 219. 10.1083/jcb.201908212.
15. Boutelle AM, and Attardi LD (2021). p53 and Tumor Suppression: It Takes a Network. Trends Cell Biol 31, 298–310. 10.1016/j.tcb.2020.12.011. [PubMed: 33518400]
16. Tarangelo A, Magtanong L, Bieging-Rolett KT, Li Y, Ye J, Attardi LD, and Dixon SJ (2018). p53 Suppresses Metabolic Stress-Induced Ferroptosis in Cancer Cells. Cell Rep 22, 569–575. 10.1016/j.celrep.2017.12.077. [PubMed: 29346757]
17. Tarangelo A, Rodencal J, Kim JT, Magtanong L, Long JZ, and Dixon SJ (2022). Nucleotide biosynthesis links glutathione metabolism to ferroptosis sensitivity. Life Sci Alliance 5. 10.26508/lsa.202101157.
18. Kuganesan N, Dlamini S, Tillekeratne LMV, and Taylor WR (2021). Tumor suppressor p53 promotes ferroptosis in oxidative stress conditions independent of modulation of ferroptosis by p21, CDKs, RB, and E2F. J Biol Chem 297, 101365. 10.1016/j.jbc.2021.101365. [PubMed: 34728216]
19. Wang ME, Chen J, Lu Y, Bawcom AR, Wu J, Ou J, Asara JM, Armstrong AJ, Wang Q, Li L, et al. (2023). RB1-deficient prostate tumor growth and metastasis are vulnerable to ferroptosis induction via the E2F/ACSL4 axis. J Clin Invest. 10.1172/JCI166647.
20. Venkatesh D, Stockwell BR, and Prives C (2020). p21 can be a barrier to ferroptosis independent of p53. Aging (Albany NY) 12, 17800–17814. 10.18632/aging.103961. [PubMed: 32979260]
21. Minami JK, Morrow D, Bayley NA, Fernandez EG, Salinas JJ, Tse C, Zhu H, Su B, Plawat R, Jones A, et al. (2023). CDKN2A deletion remodels lipid metabolism to prime glioblastoma for ferroptosis. Cancer Cell 41, 1048–1060 e1049. 10.1016/j.ccell.2023.05.001. [PubMed: 37236196]
22. Forcina GC, Conlon M, Wells A, Cao JY, and Dixon SJ (2017). Systematic Quantification of Population Cell Death Kinetics in Mammalian Cells. Cell Syst 4, 600–610 e606. 10.1016/j.cels.2017.05.002. [PubMed: 28601558]
23. Le Pen J, Maillet L, Sarosiek K, Vuillier C, Gautier F, Montessuit S, Martinou JC, Letai A, Braun F, and Juin PP (2016). Constitutive p53 heightens mitochondrial apoptotic priming and favors cell death induction by BH3 mimetic inhibitors of BCL-xL. Cell Death Dis 7, e2083. 10.1038/cddis.2015.400. [PubMed: 26844698]

24. Venkatesh D, O'Brien NA, Zandkarimi F, Tong DR, Stokes ME, Dunn DE, Kengmana ES, Aron AT, Klein AM, Csuka JM, et al. (2020). MDM2 and MDMX promote ferroptosis by PPARalpha-mediated lipid remodeling. Genes Dev 34, 526–543. 10.1101/gad.334219.119. [PubMed: 32079652]
25. Xie Y, Zhu S, Song X, Sun X, Fan Y, Liu J, Zhong M, Yuan H, Zhang L, Billiar TR, et al. (2017). The Tumor Suppressor p53 Limits Ferroptosis by Blocking DPP4 Activity. Cell Rep 20, 1692–1704. 10.1016/j.celrep.2017.07.055. [PubMed: 28813679]
26. Rubin SM, Sage J, and Skotheim JM (2020). Integrating Old and New Paradigms of G1/S Control. Mol Cell 80, 183–192. 10.1016/j.molcel.2020.08.020. [PubMed: 32946743]
27. O'Leary B, Finn RS, and Turner NC (2016). Treating cancer with selective CDK4/6 inhibitors. Nat Rev Clin Oncol 13, 417–430. 10.1038/nrclinonc.2016.26. [PubMed: 27030077]
28. Chaikovsky AC, Li C, Jeng EE, Loebell S, Lee MC, Murray CW, Cheng R, Demeter J, Swaney DL, Chen SH, et al. (2021). The AMBRA1 E3 ligase adaptor regulates the stability of cyclin D. Nature 592, 794–798. 10.1038/s41586-021-03474-7. [PubMed: 33854239]
29. Randolph JT, O'Connor MJ, Han F, Hutchins CW, Siu YA, Cho M, Zheng Y, Hickson JA, Markley JL, Manaves V, et al. (2023). Discovery of a Potent Chloroacetamide GPX4 Inhibitor with Bioavailability to Enable Target Engagement in Mice, a Potential Tool Compound for Inducing Ferroptosis In Vivo. J Med Chem 66, 3852–3865. 10.1021/acs.jmedchem.2c01415. [PubMed: 36877935]
30. Rodencal J, and Dixon SJ (2023). A tale of two lipids: Lipid unsaturation commands ferroptosis sensitivity. Proteomics 23, e2100308. 10.1002/pmic.202100308. [PubMed: 36398995]
31. Sherr CJ, Beach D, and Shapiro GI (2016). Targeting CDK4 and CDK6: From Discovery to Therapy. Cancer Discov 6, 353–367. 10.1158/2159-8290.CD-15-0894. [PubMed: 26658964]
32. Zhang W, and Liu HT (2002). MAPK signal pathways in the regulation of cell proliferation in mammalian cells. Cell Res 12, 9–18. 10.1038/sj.cr.7290105. [PubMed: 11942415]
33. Bracken AP, Ciro M, Cocito A, and Helin K (2004). E2F target genes: unraveling the biology. Trends Biochem Sci 29, 409–417. 10.1016/j.tibs.2004.06.006. [PubMed: 15362224]
34. Rees MG, Seashore-Ludlow B, Cheah JH, Adams DJ, Price EV, Gill S, Javaid S, Coletti ME, Jones VL, Bodycombe NE, et al. (2016). Correlating chemical sensitivity and basal gene expression reveals mechanism of action. Nat Chem Biol 12, 109–116. 10.1038/nchembio.1986. [PubMed: 26656090]
35. Fischer M, Schwarz R, Riege K, DeCaprio JA, and Hoffmann S (2022). TargetGeneReg 2.0: a comprehensive web-atlas for p53, p63, and cell cycle-dependent gene regulation. NAR Cancer 4, zcac009. 10.1093/narcan/zcac009. [PubMed: 35350773]
36. Gijon MA, Riekhof WR, Zarini S, Murphy RC, and Voelker DR (2008). Lysophospholipid acyltransferases and arachidonate recycling in human neutrophils. J Biol Chem 283, 30235–30245. 10.1074/jbc.M806194200. [PubMed: 18772128]
37. Liang D, Feng Y, Zandkarimi F, Wang H, Zhang Z, Kim J, Cai Y, Gu W, Stockwell BR, and Jiang X (2023). Ferroptosis surveillance independent of GPX4 and differentially regulated by sex hormones. Cell. 10.1016/j.cell.2023.05.003.
38. Yi J, Zhu J, Wu J, Thompson CB, and Jiang X (2020). Oncogenic activation of PI3K-AKT-mTOR signaling suppresses ferroptosis via SREBP-mediated lipogenesis. Proc Natl Acad Sci U S A 117, 31189–31197. 10.1073/pnas.2017152117. [PubMed: 33229547]
39. Tesfay L, Paul BT, Konstorum A, Deng Z, Cox AO, Lee J, Furdui CM, Hegde P, Torti FM, and Torti SV (2019). Stearoyl-CoA Desaturase 1 Protects Ovarian Cancer Cells from Ferroptotic Cell Death. Cancer Res 79, 5355–5366. 10.1158/0008-5472.CAN-19-0369. [PubMed: 31270077]
40. Ubellacker JM, Tasdogan A, Ramesh V, Shen B, Mitchell EC, Martin-Sandoval MS, Gu Z, McCormick ML, Durham AB, Spitz DR, et al. (2020). Lymph protects metastasizing melanoma cells from ferroptosis. Nature 585, 113–118. 10.1038/s41586-020-2623-z. [PubMed: 32814895]
41. Wu S, Mao C, Kondiparthi L, Poyurovsky MV, Olszewski K, and Gan B (2022). A ferroptosis defense mechanism mediated by glycerol-3-phosphate dehydrogenase 2 in mitochondria. Proc Natl Acad Sci U S A 119, e2121987119. 10.1073/pnas.2121987119. [PubMed: 35749365]

42. Santos A, Wernersson R, and Jensen LJ (2015). Cyclebase 3.0: a multi-organism database on cell-cycle regulation and phenotypes. Nucleic Acids Res 43, D1140–1144. 10.1093/nar/gku1092. [PubMed: 25378319]
43. Ma Y, Schroder DC, Nenkov M, Rizwan MN, Abubrig M, Sonnemann J, Murrieta-Coxca JM, Morales-Prieto DM, Westermann M, Gassler N, and Chen Y (2021). Epithelial Membrane Protein 2 Suppresses Non-Small Cell Lung Cancer Cell Growth by Inhibition of MAPK Pathway. Int J Mol Sci 22. 10.3390/ijms22062944.
44. Hishikawa D, Shindou H, Kobayashi S, Nakanishi H, Taguchi R, and Shimizu T (2008). Discovery of a lysophospholipid acyltransferase family essential for membrane asymmetry and diversity. Proc Natl Acad Sci U S A 105, 2830–2835. 10.1073/pnas.0712245105. [PubMed: 18287005]
45. Valentine WJ, Yanagida K, Kawana H, Kono N, Noda NN, Aoki J, and Shindou H (2022). Update and nomenclature proposal for mammalian lysophospholipid acyltransferases, which create membrane phospholipid diversity. J Biol Chem 298, 101470. 10.1016/j.jbc.2021.101470. [PubMed: 34890643]
46. Dauwerse JG, de Vries BB, Wouters CH, Bakker E, Rappold G, Mortier GR, Breuning MH, and Peters DJ (2007). A t(4;6)(q12;p23) translocation disrupts a membrane-associated O-acetyl transferase gene (MBOAT1) in a patient with a novel brachydactyly-syndactyly syndrome. Eur J Hum Genet 15, 743–751. 10.1038/sj.ejhg.5201833. [PubMed: 17440500]
47. Mozaffari K, Mekonnen M, Harary M, Lum M, Aguirre B, Chandla A, Wadehra M, and Yang I (2023). Epithelial membrane protein 2 (EMP2): A systematic review of its implications in pathogenesis. Acta Histochem 125, 151976. 10.1016/j.acthis.2022.151976. [PubMed: 36455339]
48. Gaud C, B CS, Nguyen A, Fedorova M, Ni Z, O'Donnell VB, Wakelam MJO, Andrews S, and Lopez-Clavijo AF (2021). BioPAN: a web-based tool to explore mammalian lipidome metabolic pathways on LIPID MAPS. F1000Res 10, 4. 10.12688/f1000research.28022.2. [PubMed: 33564392]
49. Jiang C, Pandey A, Chen R, Kalita B, Duraiswamy AJ (2020) COMPOUNDS WITH FERROPTOSIS INDUCING ACTIVITY AND METHODS OF THEIR USE. patent application PCT /US2020/020150.
50. Friedmann Angeli JP, Schneider M, Proneth B, Tyurina YY, Tyurin VA, Hammond VJ, Herbach N, Aichler M, Walch A, Eggenhofer E, et al. (2014). Inactivation of the ferroptosis regulator Gpx4 triggers acute renal failure in mice. Nat Cell Biol 16, 1180–1191. 10.1038/ncb3064. [PubMed: 25402683]
51. Jiang L, Kon N, Li T, Wang SJ, Su T, Hibshoosh H, Baer R, and Gu W (2015). Ferroptosis as a p53-mediated activity during tumour suppression. Nature 520, 57–62. 10.1038/nature14344. [PubMed: 25799988]
52. Hangauer MJ, Viswanathan VS, Ryan MJ, Bole D, Eaton JK, Matov A, Galeas J, Dhruv HD, Berens ME, Schreiber SL, et al. (2017). Drug-tolerant persister cancer cells are vulnerable to GPX4 inhibition. Nature 551, 247–250. 10.1038/nature24297. [PubMed: 29088702]
53. Kalkavan H, Chen MJ, Crawford JC, Quarato G, Fitzgerald P, Tait SWG, Goding CR, and Green DR (2022). Sublethal cytochrome c release generates drug-tolerant persister cells. Cell 185, 3356–3374 e3322. 10.1016/j.cell.2022.07.025. [PubMed: 36055199]
54. Tousignant KD, Rockstroh A, Poad BLJ, Talebi A, Young RSE, Taherian Fard A, Gupta R, Zang T, Wang C, Lehman ML, et al. (2020). Therapy-induced lipid uptake and remodeling underpin ferroptosis hypersensitivity in prostate cancer. Cancer Metab 8, 11. 10.1186/s40170-020-00217-6. [PubMed: 32577235]
55. Oren Y, Tsabar M, Cuoco MS, Amir-Zilberstein L, Cabanos HF, Hutter JC, Hu B, Thakore PI, Tabaka M, Fulco CP, et al. (2021). Cycling cancer persister cells arise from lineages with distinct programs. Nature 596, 576–582. 10.1038/s41586-021-03796-6. [PubMed: 34381210]
56. Zou Y, Henry WS, Ricq EL, Graham ET, Phadnis VV, Maretich P, Paradkar S, Boehnke N, Deik AA, Reinhardt F, et al. (2020). Plasticity of ether lipids promotes ferroptosis susceptibility and evasion. Nature 585, 603–608. 10.1038/s41586-020-2732-8. [PubMed: 32939090]
57. Knudsen ES, Hutcheson J, Vail P, and Witkiewicz AK (2017). Biological specificity of CDK4/6 inhibitors: dose response relationship, in vivo signaling, and composite response signature. Oncotarget 8, 43678–43691. 10.18632/oncotarget.18435. [PubMed: 28620137]

58. Yang WH, Ding CC, Sun T, Rupprecht G, Lin CC, Hsu D, and Chi JT (2019). The Hippo Pathway Effector TAZ Regulates Ferroptosis in Renal Cell Carcinoma. Cell Rep 28, 2501–2508 e2504. 10.1016/j.celrep.2019.07.107. [PubMed: 31484063]

59. Qin Y, Fu M, Takahashi M, Iwanami A, Kuga D, Rao RG, Sudhakar D, Huang T, Kiyohara M, Torres K, et al. (2014). Epithelial membrane protein-2 (EMP2) activates Src protein and is a novel therapeutic target for glioblastoma. J Biol Chem 289, 13974–13985. 10.1074/jbc.M113.543728. [PubMed: 24644285]

60. Dillard C, Kiyohara M, Mah V, McDermott SP, Bazzoun D, Tsui J, Chan AM, Haddad G, Pellegrini M, Chang YL, et al. (2020). EMP2 Is a Novel Regulator of Stemness in Breast Cancer Cells. Mol Cancer Ther 19, 1682–1695. 10.1158/1535-7163.MCT-19-0850. [PubMed: 32451329]

61. Conlon M, Poltorack CD, Forcina GC, Armenta DA, Mallais M, Perez MA, Wells A, Kahanu A, Magtanong L, Watts JL, et al. (2021). A compendium of kinetic modulatory profiles identifies ferroptosis regulators. Nat Chem Biol. 10.1038/s41589-021-00751-4.

62. Hendricks JM, Doubravsky CE, Wehri E, Li Z, Roberts MA, Deol KK, Lange M, Lasheras-Otero I, Momper JD, Dixon SJ, et al. (2023). Identification of structurally diverse FSP1 inhibitors that sensitize cancer cells to ferroptosis. Cell Chem Biol. 10.1016/j.chembiol.2023.04.007.

63. Inde Z, Rodencal J, and Dixon SJ (2021). Quantification of drug-induced fractional killing using high-throughput microscopy. STAR Protoc 2, 100300. 10.1016/j.xpro.2021.100300. [PubMed: 33532743]

64. Inde Z, Forcina GC, Denton K, and Dixon SJ (2020). Kinetic Heterogeneity of Cancer Cell Fractional Killing. Cell Rep 32, 107845. 10.1016/j.celrep.2020.107845. [PubMed: 32640215]

65. Barupal DK, Zhang Y, Shen T, Fan S, Roberts BS, Fitzgerald P, Wancewicz B, Valdiviez L, Wohlgemuth G, Byram G, et al. (2019). A Comprehensive Plasma Metabolomics Dataset for a Cohort of Mouse Knockouts within the International Mouse Phenotyping Consortium. Metabolites 9. 10.3390/metabo9050101.

66. Koch J, Lackner K, Wohlfarter Y, Sailer S, Zschocke J, Werner ER, Watschinger K, and Keller MA (2020). Unequivocal Mapping of Molecular Ether Lipid Species by LC-MS/MS in Plasmalogen-Deficient Mice. Anal Chem 92, 11268–11276. 10.1021/acs.analchem.0c01933. [PubMed: 32692545]

67. Lange M, Angelidou G, Ni Z, Criscuolo A, Schiller J, Bluher M, and Fedorova M (2021). AdipoAtlas: A reference lipidome for human white adipose tissue. Cell Rep Med 2, 100407. 10.1016/j.xcrm.2021.100407. [PubMed: 34755127]

68. Koelmel JP, Kroeger NM, Gill EL, Ulmer CZ, Bowden JA, Patterson RE, Yost RA, and Garrett TJ (2017). Expanding Lipidome Coverage Using LC-MS/MS Data-Dependent Acquisition with Automated Exclusion List Generation. J Am Soc Mass Spectrom 28, 908–917. 10.1007/s13361-017-1608-0. [PubMed: 28265968]

69. Xia J, Psychogios N, Young N, and Wishart DS (2009). MetaboAnalyst: a web server for metabolomic data analysis and interpretation. Nucleic Acids Res 37, W652–660. 10.1093/nar/gkp356. [PubMed: 19429898]

70. Smith AR (1979). Tint fill. ACM SIGGRAPH Computer Graphics 13, 276–283. 10.1145/965103.

Highlights:

- p53 stabilization and CDK4/6 inhibition sensitize cells to direct GPX4 inhibitors
- p53 stabilization and CDK4/6 inhibition reduce *MBOAT1* and *EMP2* expression
- EMP2 loss sensitizes cells to GPX4 inhibitors by altering lipid metabolism
- An orally bioavailable GPX4 inhibitor is active in vivo

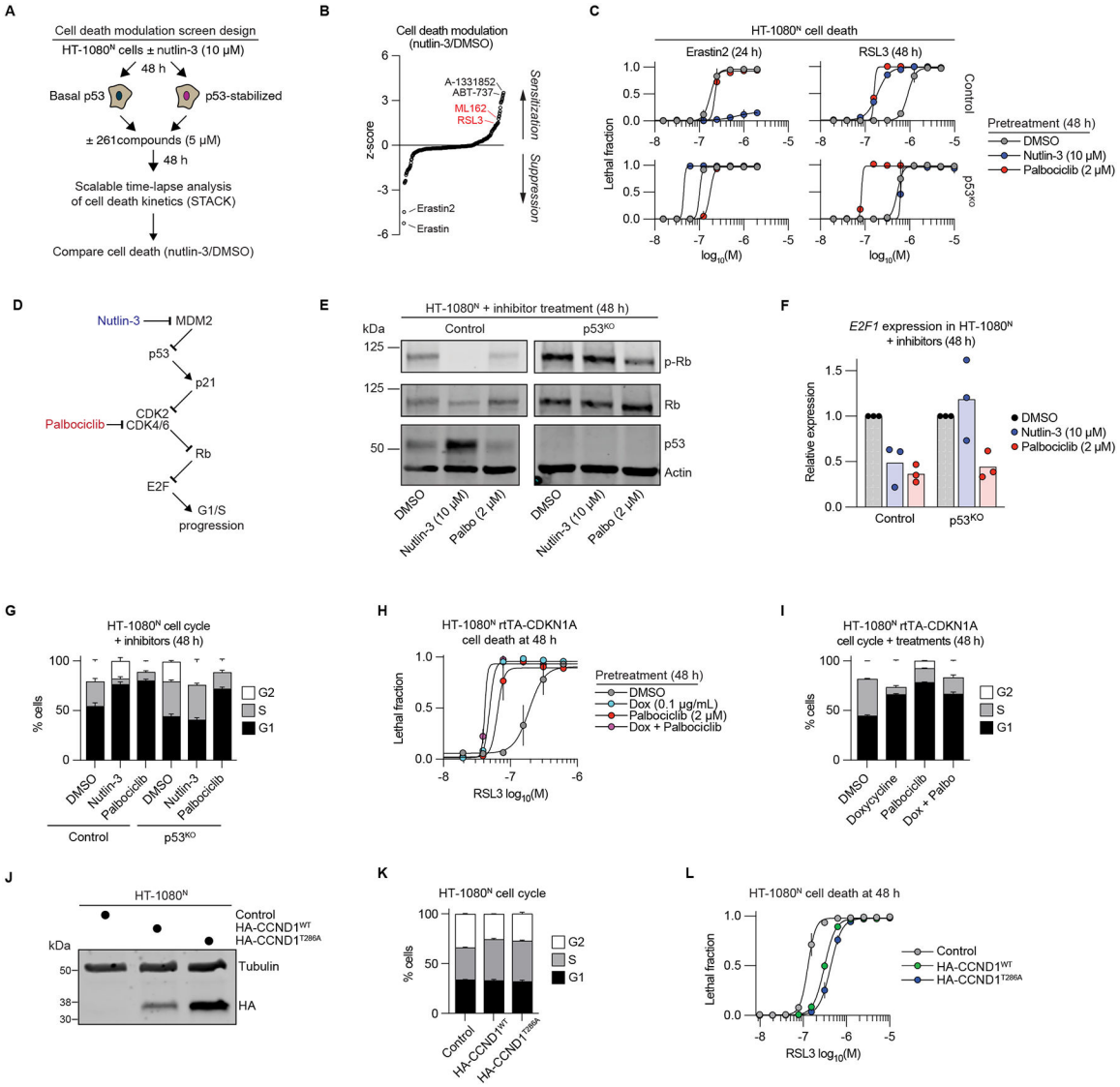

Figure 1. p53 stabilization sensitizes to GPX4 inhibitors.

(A) Outline of the small molecule phenotypic screen.

(B) Cell death modulation z-scores for HT-1080^{N} cells pretreated ± nutlin-3 (10 μM, 48 h) then treated ± 261 bioactive compounds (5 μM). The screen was repeated three times and z-scored mean values are shown. Compounds of interest are highlighted.

(C) Cell death measured by imaging following pretreatment.

(D) Outline of the CDK-Rb-E2F cell cycle pathway and associated inhibitors.

(E) Protein abundance determined by immunoblotting. Blots are representative of three experiments. Palbo, palbociclib.

(F) Relative mRNA expression determined by reverse transcription and quantitative polymerase chain reaction (RT-qPCR) analysis. Individual datapoints from independent experiments are shown.

(G) Cell cycle phase determined by propidium iodide (PI) staining and flow cytometry. Nutlin-3 was used at 10 μM and palbociclib at 2 μM.

(H) Cell death measured by imaging following pretreatment. Dox, doxycycline.
(I) Cell cycle phase determined by PI staining and flow cytometry. Dox was used at 0.1 μg/mL, palbociclib (Palbo) at 2 μM.
(J) Protein abundance determined by immunoblotting. Blot is representative of three experiments.
(K) Cell cycle phase determined by PI staining and flow cytometry in stable cell lines expressing the indicated constructs.
(L) Cell death measured by imaging in stable cell lines expressing the indicated constructs.
Data in (C), (G-I), (K) and (L) represent mean ± SD from three independent experiments.

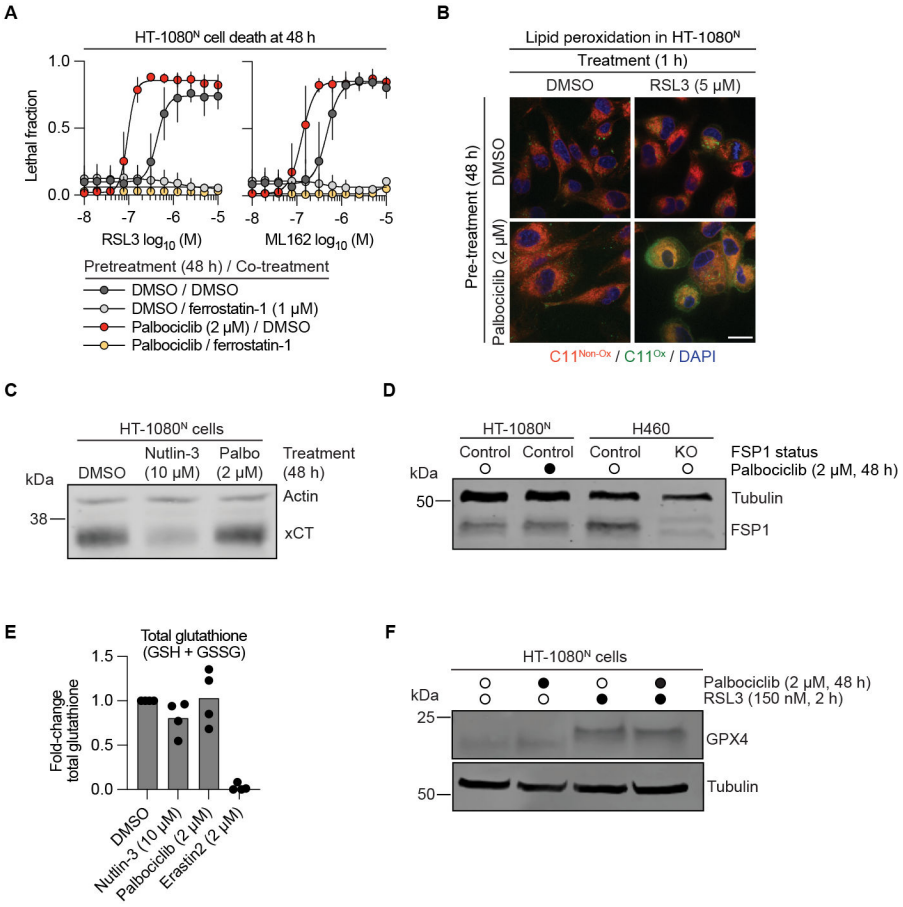

Figure 2. GPX4 inhibitor sensitization involves increased lipid peroxidation.

(A) Cell death measured by imaging following pretreatment. Data represent mean ± SD from three independent experiments.

(B) C11 BODIPY 581/591 (C11) imaging by confocal microscopy. Non-ox: non-oxidized, Ox: oxidized. Scale bar = 20 μm. Images are representative of three experiments.

(C) Protein abundance determined by immunoblotting. Palbo, palbociclib.

(D) Protein abundance determined by immunoblotting. H460 Control and *FSP1* gene-disrupted (KO) cell lines are included as an anti-FSP1 antibody control.

(E) Relative total glutathione levels determined using Ellman's reagent. Nutlin-3 and palbociclib treatments were for 48 h. Erastin2 treatment (8 h) is a positive control for glutathione depletion. Individual data points from four independent experiments are shown.

(F) Protein abundance and migration determined by immunoblotting. Cells were pretreated ± palbociclib for 48 h before treatment ± RSL3.

Blots in (C), (D) and (F) are representative of three independent experiments.

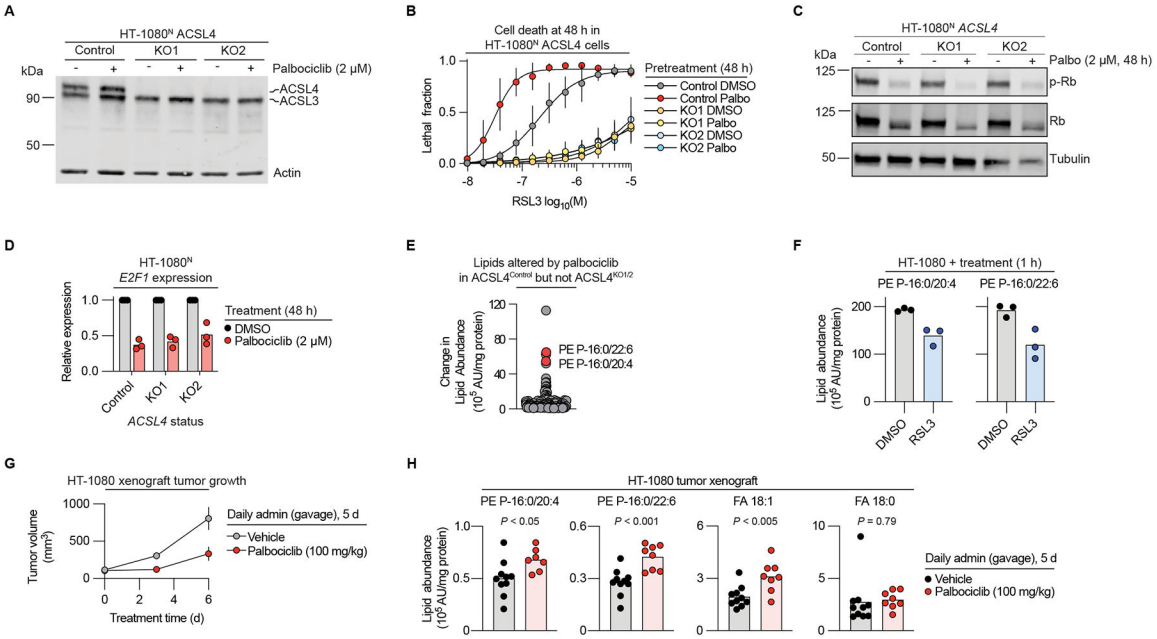

Figure 3. Altered lipid peroxidation sensitivity requires ACSL4.

(A) Protein abundance determined by immunoblotting. KO1, gene-disrupted cell line 1. KO2, gene-disrupted cell line 2. Cell line genotypes and protein phenotypes have been reported previously.[8,12]

(B) Cell death measured by imaging following pretreatment. Results represent mean ± SD from three independent experiments.

(C) Protein abundance determined by immunoblotting. Palbo: palbociclib.

(D) Relative *E2F1* expression determined by reverse transcription and quantitative polymerase chain reaction (RT-qPCR) analysis.

(E) Differentially abundant (FDR $q < 0.05$) lipids following palbociclib (2 μM, 48 h) treatment in Control versus ACSL4$^{KO1/2}$ cell lines, as determined by liquid chromatography coupled to mass spectrometry (LC-MS) analysis (see Materials and Methods). Each dot represents one species and is the average of five or six independent cultures examined in parallel. Lipids confirmed by MS/MS analysis are indicated. AU, arbitrary units.

(F) Analysis of lipid abundance by LC-MS. RSL3 was used at 1 μM. AU, arbitrary units.

(G) Analysis of HT-1080 tumor xenografts growth. Tumors were allowed to grow to an average size of ~100 mm^3, then mice were treated ± palbociclib daily for 5 days (tumors were harvested on day 6 for further analysis). Data represent mean ± SEM (n = 8 or 10 tumors per condition).

(H) Lipid abundance following treatment, as determined by liquid chromatography coupled to mass spectrometry (LC-MS) analysis. Data from individual tumors is shown. Two-tailed Student's t-test was used to compare mean differences between groups. AU, arbitrary units.

Blots in (A) and (C) are representative of three experiments. Individual datapoints from separate experiments are shown in (D) and (F).

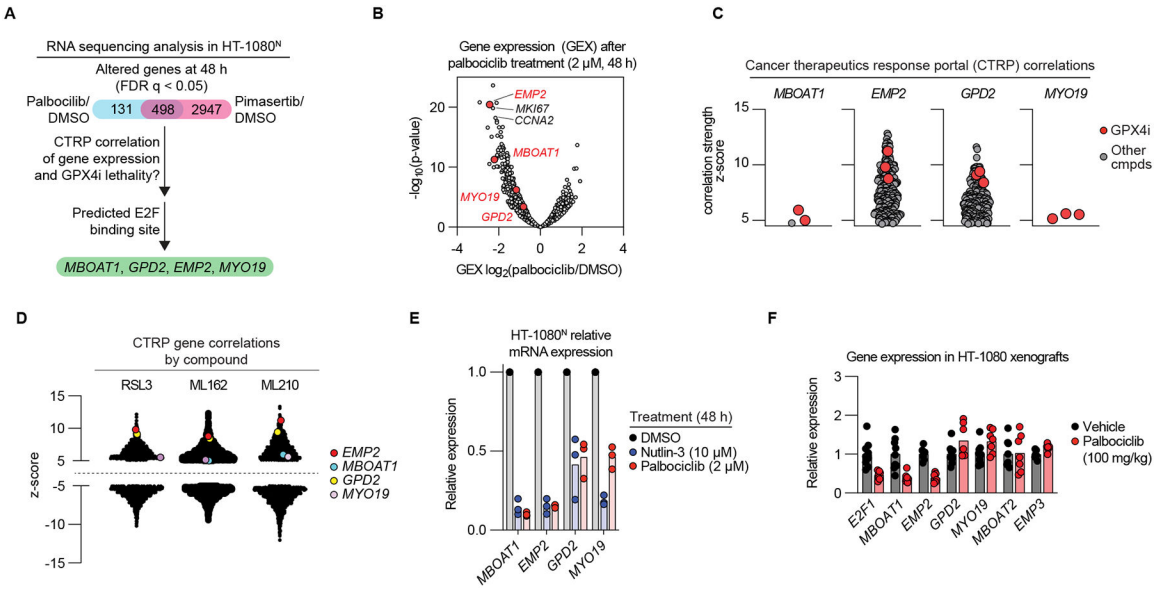

Figure 4. Identification of cell cycle-regulated genes associated with ferroptosis.

(A) Overview of the pipeline used to identify candidate regulators of ferroptosis sensitivity. CTRP, Cancer Therapeutics Response Portal.

(B) RNA-sequencing. Labeled red points are from (A)

(C-D) Data from the CTRP database correlating compound sensitivity and basal gene expression. Points in (C) represent an individual compounds correlated with the labeled gene. Points in (D) represent individual genes correlated with the labeled compound.

(E) Relative mRNA expression determined by reverse transcription and quantitative polymerase chain reaction (RT-qPCR) analysis. Individual datapoints from separate experiments are shown.

(F) Relative mRNA expression determined by RT-qPCR analysis from tumor xenografts harvested previously. Individual datapoints represent separate xenograft tumors. Data is normalized to mean ΔΔCT values of vehicle control for each gene.

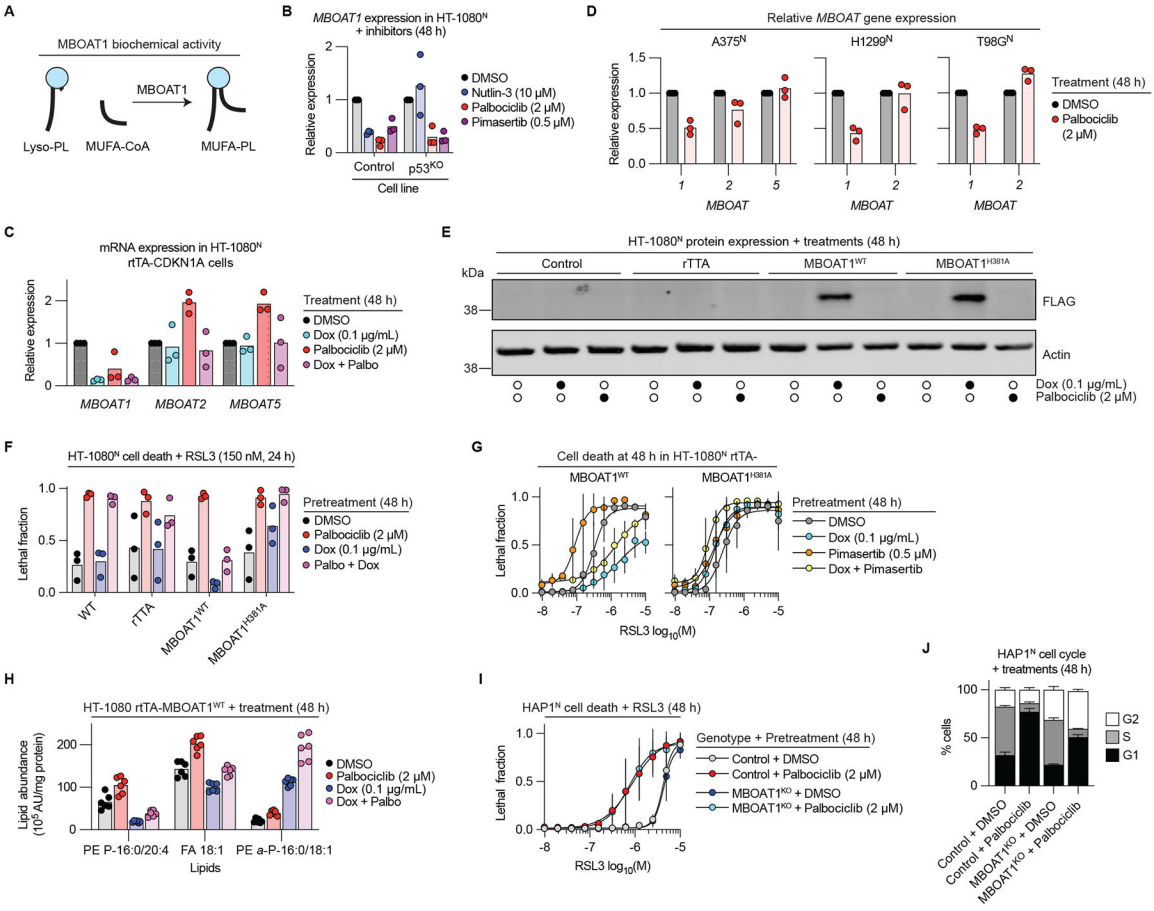

Figure 5. MBOAT1 can regulate ferroptosis sensitivity.

(A) Cartoon schematic of MBOAT1 function.

(B-D) Relative mRNA expression determined by reverse transcription and quantitative polymerase chain reaction (RT-qPCR) analysis. Dox, doxycycline.

(E) Protein abundance determined by immunoblotting. Blots are representative of three experiments.

(F,G) Cell death measured by imaging following pretreatment.

(H) Lipid abundance following treatment, as determined by liquid chromatography coupled to mass spectrometry (LC-MS) analysis. AU, arbitrary units.

(I) Cell death measured by imaging following pretreatment.

(J) Cell cycle phase determined by propidium iodide (PI) staining and flow cytometry. Palbociclib was used at 2 μM.

Individual datapoints from independent experiments are shown in (B-D), (F) and (H). Data in (G), (I) and (J) represent mean ± SD from three independent experiments.

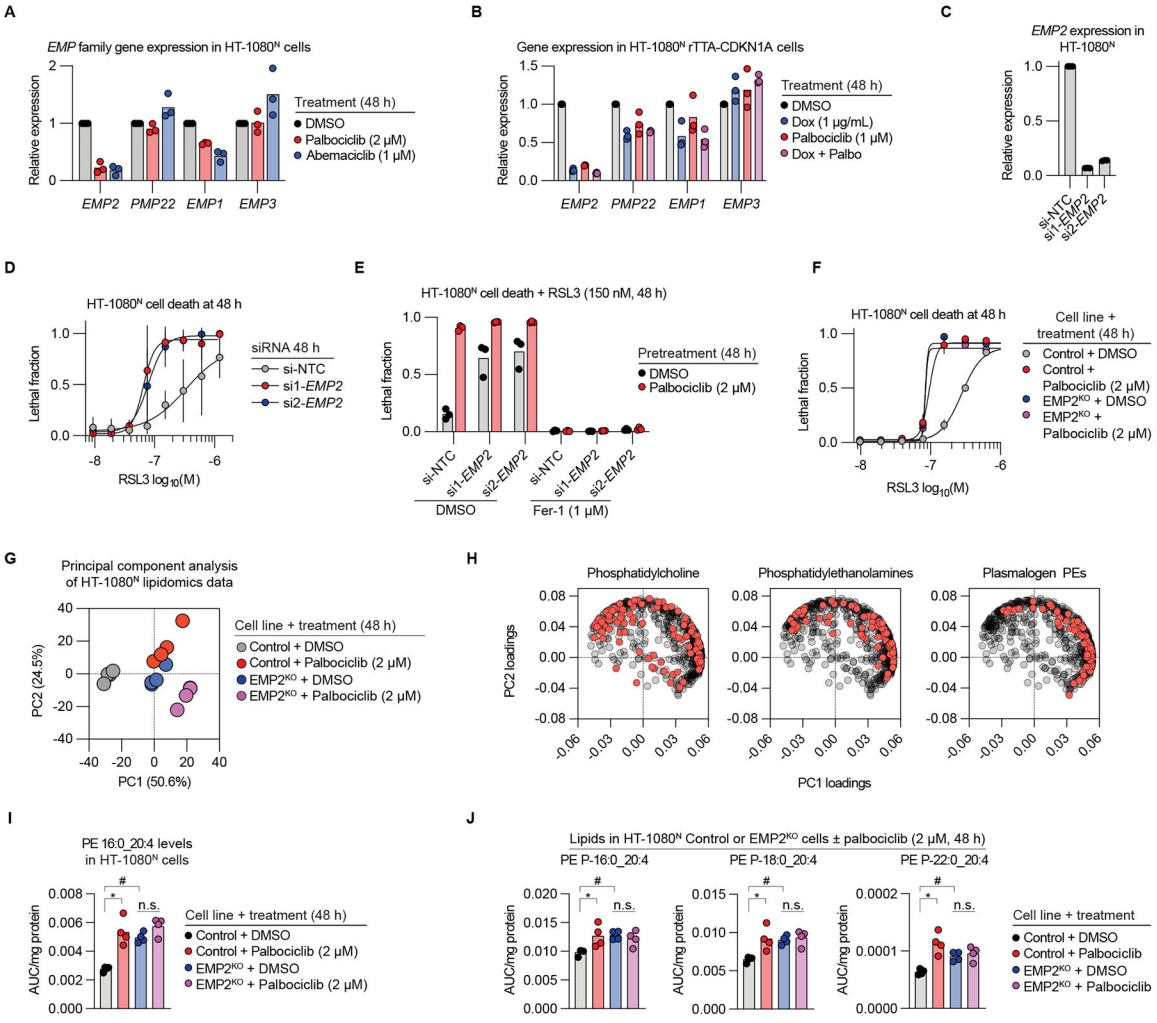

Figure 6. EMP2 regulates ferroptosis sensitivity.

(A-C) Relative mRNA expression determined by reverse transcription and quantitative polymerase chain reaction (RT-qPCR) analysis. Dox, doxycycline. si, short interfering RNA. NTC, non-targeting control.

(D-F) Cell death measured by imaging following pretreatment. Fer-1, ferrostatin-1.

(G) Principal component analysis (PCA) scores plot. Each point represents one sample.

(H) PCA loadings plots. Each red point belongs to the lipid class labeled in the graph title.

(I-J) Lipid abundance following treatment, as determined by liquid chromatography coupled to mass spectrometry (LC-MS) analysis. *Indicates FDR q < 0.05. #Indicates FDR q < 0.01. AUC, area under the curve.

Individual datapoints from three (A-C), (E), or four (I) and (J) independent experiments are shown. Results in (D), (F) represent mean ± SD from three independent experiments.

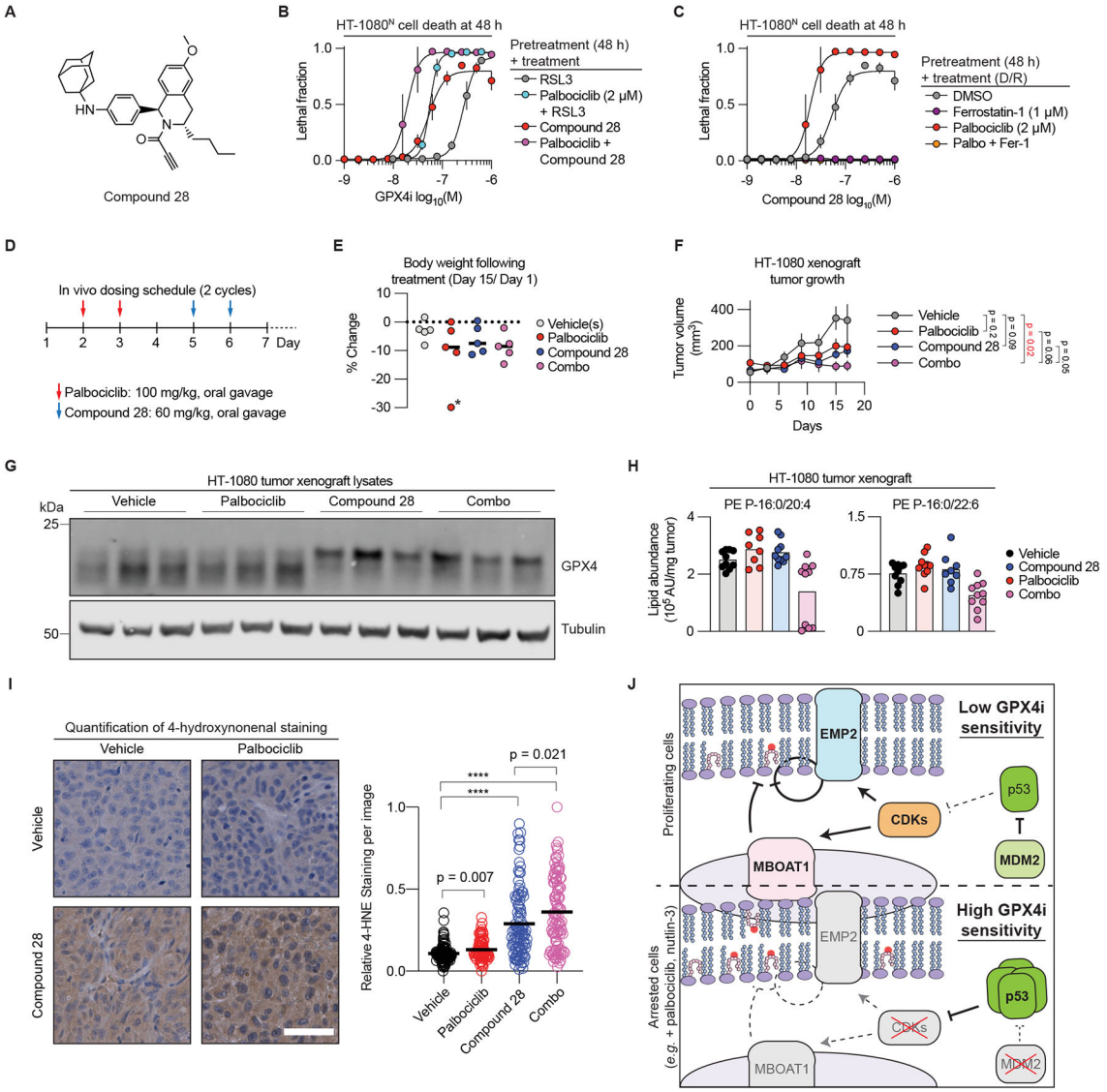

Figure 7. CDK inhibition modulates ferroptosis in vivo.

(A) Structure of compound 28.

(B, C) Cell death measured by imaging following pretreatment. Note that the compound 28 data in the DMSO and palbociclib pre-treatments conditions (without ferrostatin-1) in (C) are the same as shown in (B) as this was all part of one larger experiment. Data represent mean ± SD from three independent experiments.

(D) A dosing schedule for the combination of palbociclib and compound 28.

(E) Change in mouse body weight from the start to the end of the xenograft study. Body weight was measured every 3 d. Each dot represents data from one animal. Note: two xenograft tumors were implanted per animal, one on each flank. *One animal that lost body weight rapidly between days 12 and 15 was not included in the subsequent analysis.

(F) Tumor xenograft size over time, determined by caliper measurements. Data are mean ± SEM, n = 8-10 tumors per condition. p-values indicate the results of 2-tailed t-tests of tumor volumes on day 17.

(G) Protein abundance and migration determined by immunoblotting. Three randomly selected xenograft tumors were used from each condition.
(H) Lipid abundance measured by liquid chromatography coupled to mass spectrometry. Individual datapoints from 8 or 10 individual tumors. AU, arbitrary units.
(I) Staining and quantification of the lipid peroxidation breakdown product 4-hydroxynonenal (4-HNE) in tumor xenografts. Scale bar = 50 μm. In the graph, each dot represents quantified intensity from one region of interest (ROI) from a xenograft tissue section. Ten ROIs/xenograft sample were acquired. Horizontal black bars indicate mean for each condition. ****$p < 10^{-10}$, Student's t-test (2-tailed).
(J) Model of the proposed mechanism.

Key resources table

REAGENT or RESOURCE	SOURCE	IDENTIFIER
Antibodies		
anti-ACSL4	Proteintech	Cat# 22401-1-AP RRID:AB_2832995
anti-Actin (C4)	Santa Cruz Biotechnology	Cat# sc-47778 RRID:AB_626632
anti-Tubulin (DM1A)	Thermo Fisher Scientific	Cat# MS581P1
anti-p21 (12D1)	Cell Signaling Technology	Cat# #2947 RRID:AB_823586
anti-Rb (G3-245)	BD Biosciences	Cat# 554136 RRID:AB_395259
anti-phospho-Rb Ser807/811 (D2OB12)	Cell Signaling Technologies	Cat #8516 RRID:AB_11178658
anti-p53 (DO-1)	Santa Cruz Biotechnology	Cat# sc-126 RRID:AB_628082
anti-GPX4	Abcam	Cat# ab41787 RRID:AB_941790
anti-GPX4 (EPNCIR144)	Abcam	Cat# 125066 RRID:AB_10973901
anti-eIF4E (P-2)	Santa Cruz Biotechnology	Cat# sc-9976 RRID:AB_627502
anti-xCT (D2M7A)	Cell Signaling Technology	Cat# 12691 RRID:AB_2687474
anti-FLAG	Abcam	Cat# ab1257 RRID:AB_299216
anti-HA tag (C29F4)	Cell Signaling Technology	Cat# 3724 RRID:AB_1549585
anti-FSP1	Proteintech	Cat# 20886-1-AP RRID:AB_2878756
IRDye 680LT Donkey anti-Goat IgG	Licor	Cat# 926-68024 RRID:AB_10706168
IRDye® 800CW Donkey anti-Rabbit IgG	Licor	Cat# 926-32213 RRID:AB_621848
IRDye® 800CW Donkey anti-Mouse IgG	Licor	Cat# 926-32212 RRID:AB_621847
IRDye® 680LT Donkey anti-Rabbit IgG	Licor	Cat# 926-68023 RRID:AB_10706167
IRDye® 680LT Donkey anti-Mouse IgG	Licor	Cat# 926-68022 RRID:AB_10715072
anti-4-hydroxynonenol (IHC)	Abcam	Cat# ab46545 RRID:AB_722490
KI67 (IHC)	Proteintech	Cat# 27309-1-AP RRID:AB_2756525
BT goat anti-rabbit secondary antibody	Abcam	Cat# ab64256 RRID:AB_2661852
streptavidin-HRP tertiary antibody	Thermo Fisher Scientific	Cat# N100
Bacterial and virus strains		
NucLight Red lentivirus reagent (EF1a, Puro) Nuclear-localized mKate2 (Nuc::mKate2)	Essen BioSciences	Cat# 4265

REAGENT or RESOURCE	SOURCE	IDENTIFIER
Biological samples		
N/A		
Chemicals, peptides, and recombinant proteins		
ML162	Acme	N/A
Erastin2	Cayman Chemicals	Cat# 27087
Deferoxamine	Cayman Chemicals	Cat# 14595
Palbociclib	Selleck Chemicals	Cat# S1116
Pimasertib	Selleck Chemicals	Cat# S1475
1*S*,3*R*-RSL3	Selleck Chemicals	Cat# S8155 CAS: 1219810-16-8
Doxycycline	Sigma-Aldrich	Cat# D3447
ML210	Sigma-Aldrich	Cat# SML0521 CAS: 1360705-96-9
Ferrostatin-1	Sigma-Aldrich	Cat# SML0583 AS: 347174-05-4
Propidium iodide	Sigma-Aldrich	Cat# P4170
Abemaciclib	MedChem Express	Cat# HY-16297A
Bortezomib	Thermo Fisher Scientific	Cat# NC0587961 CAS: 179324-69-7
Q-VD-OPh	Thermo Fisher Scientific	Cat# OPH00101M
Etoposide	Thermo Fisher Scientific	Cat# 12-261-00
DAPI	Thermo Fisher Scientific	Cat# D1306
C11 BODIPY 581/591	Thermo Fisher Scientific	Cat# D-3861
Compound 28	Ferro Therapeutics	N/A
Compound library	Selleck Chemicals	Cat# L1700
SYTOX Green	Life Technologies	Cat# S7020
Polybrene	Sigma-Aldrich	Cat# H9268-5G
Puromycin	Life Technologies	Cat# A11138-03
Lipofectamine RNAiMAX Transfection Reagent	Life Technologies	Cat # 13778075
Hoechst	Molecular Probes	Cat# H1399
Chloroform	Sigma-Aldrich	Cat# 366927
Methanol	Sigma-Aldrich	Cat# 34860-4L-R
Toluene	Sigma-Aldrich	Cat# 34866
SPLASH® LIPIDOMIX® internal standard	Avanti Polar Lipids	Cat# 330707-1EA
tert-butyl methyl ether	Sigma Aldrich	Cat# 34875-1L
Palbociclib (for *in vivo* studies)	LC Laboratories	Cat# P-7788
Critical commercial assays		
QIAshredder RNA Extraction Column Kit	Qiagen	Cat# 79654
RNeasy Plus RNA Extraction Kit	Qiagen	Cat# 74134
TaqMan Reverse Transcriptase Kit	TaqMan	Cat# N8080234
Cayman Glutathione Kit	Cayman Chemical	Cat # 703002

REAGENT or RESOURCE	SOURCE	IDENTIFIER
QIAprep Spin Miniprep Kit	Qiagen	Cat# 27106
QIAquick PCR Purification Kit	Qiagen	Cat# 28106
SYBR Green Master Mix	Life Technologies	Cat# 4367659
Gateway LR Clonase II Enzyme Mix	Thermo Fisher	Cat# 11791-020
BCA Protein Assay Kit	Thermo Fisher	Cat# 23225
Plasmid Plus Midi Kit	Qiagen	Cat# 12943
DAB chromogen	Abcam	Cat# ab64238
Deposited data		
Raw RNA sequencing data	This paper; Gene Expression Omnibus	GEO: (GSE180265)
Small molecule screening data (Data S1)	This paper; Mendeley Data	DOI: 10.17632/9zrj6vbymy.4
Lipidomic data for Control and *ACSL4* mutant cells (Data S2)	This paper; Mendeley Data	DOI: 10.17632/9zrj6vbymy.4
Processed RNA sequencing data (Data S3)	This paper; Mendeley Data	DOI: 10.17632/9zrj6vbymy.4
Lipidomic data for Control and *EMP2* mutant cells (Data S4)	This paper; Mendeley Data	DOI: 10.17632/9zrj6vbymy.4
Unprocessed western blots	This paper; Mendeley Data	DOI: 10.17632/9zrj6vbymy.4
TCGA-SARC dataset	The Cancer Genome Atlas (TCGA)	https://portal.gdc.cancer.gov/
CTRPv2 drug sensitivity data	Cancer Therapeutics Response Portal v2	https://portals.broadinstitute.org/ctrp.v2.1/
Experimental models: Cell lines		
HT-1080^{N}	Forcina et al.[23]	N/A
Caki-1^{N}	Tarangelo et al.[16]	N/A
H1299^{N}	Tarangelo et al.[16]	N/A
T98G^{N}	Forcina et al.[23]	N/A
A375^{N}	Conlon et al.[62]	N/A
HT-1080^{N} Control and p53^{KO}	Tarangelo et al.[16]	N/A
HT-1080^{N} rtTA-CDKN1A	Tarangelo et al.[16]	N/A
HT-1080^{N} Control and ACSL4$^{KO1/2}$	Magtanong et al.[8]	N/A
H460 Control and gene disrupted FSP1^{KO}	Hendricks et al.[63]	N/A
HAP1 Control and MBOAT1^{KO}	Generated by Horizon Discovery	N/A
HT-1080^{N} Control and MBOAT1^{KO1-3}	This paper	N/A
HT-1080^{N} HA-CCND1^{WT} and HT-1080^{N} HA-CCND1^{T286A}	This paper	N/A
HT-1080^{N} Control and EMP2^{KO}	This paper	N/A
786-O	ATCC	CRL-1932
MDA-MB-231	ATCC	HTB-26
Experimental models: Organisms/strains		
Mouse: NOD-*scid* IL2Rgamma^{null}	Jackson Laboratory	stock no. 005557
Oligonucleotides		
Allstars Negative Control SiRNA	Qiagen	Cat# 1027280

REAGENT or RESOURCE	SOURCE	IDENTIFIER
AllStars Hs Cell Death siRNA	Qiagen	Cat# 1027298
hs.Ri.MBOAT1.13.3	Integrated DNA Technologies	N/A
hs.Ri.EMP2.13.2	Integrated DNA Technologies	N/A
hs.Ri.EMP2.13.3	Integrated DNA Technologies	N/A
qPCR primers (see Table S1)	N/A	N/A
Recombinant DNA		
pSpCas9 (BB)-2A-GFP-sgRNA-MBOAT1	This paper	N/A
pSpCas9 (BB)-2A-GFP-sgRNA-EMP2	This paper	N/A
pLenti-CMV-Puro-MBOAT1^{WT}	This paper	N/A
pLenti-CMV-Puro-MBOAT1^{H381A}	This paper	N/A
pLenti TRE3G Dest	Laboratory of Jan Carette (Stanford School of Medicine)	N/A
Software and algorithms		
Prism 9	GraphPad Software	https://www.graphpad.com/features
Excel 16.78	Microsoft Corp.	https://www.microsoft.com/en-us/?ql=4
FlowJo	FlowJo LLC.	https://www.flowjo.com
ImageJ 1.52q	NIH	https://imagej.net/software/imagej/
R 4.0.5	The R Project for Statistical Computing	https://www.r-project.org/
RStudio 1.4.1106	Posit	https://posit.co/download/rstudio-desktop/
Python 3.10	Python Software Foundation	https://www.python.org/downloads/
PyCharm 2021.1.1	JetBrains	https://www.jetbrains.com/pycharm/download
Custom Code (4-HNE quantification)	Mendeley Data	DOI: 10.17632/9zrj6vbymy.4
xcms R package	BioConductor Version 3.16	https://bioconductor.org/packages/release/bioc/html/xcms.html
CAMERA R package	BioConductor Version 3.16	https://www.bioconductor.org/packages/release/bioc/html/CAMERA.html
Other (Plasmids)		
pMD2.G	Addgene	Cat# 12259 RRID:Addgene_12259
psPax2	Addgene	Cat# 12260 RRID:Addgene_12260
pSpCas9 (BB)-2A-GFP	Addgene	Cat# PX458